# Characterizing Asymmetric Ingression in Mammalian Epithelial Cells

Alexa Mariotti

A
Thesis
in
The Department
of
Biology

Presented in Partial Fulfillment of the Requirements for the
Degree of Master of Science (Biology) at Concordia University
Montreal, Quebec, Canada

January 2015

**CONCORDIA UNIVERSITY**

**School of Graduate Studies**

This is to certify that the thesis prepared

By: Alexa Mariotti

Entitled: Characterizing Asymmetric Ingression in Mammalian Epithelial Cells

and submitted in partial fulfillment of the requirements for the degree of

**Master of Science (Biology)**

complies with the regulations of the University and meets the accepted standards with respect to originality and quality.

Signed by the final Examining Committee:

_____Chair
Dr. Michael Sacher

_____External Examiner
Dr. Vladimir Titotrenko

_____Examiner
Dr. Catherine Bachewich

_____Examiner
Dr. Christopher Brett

_____Supervisor
Dr. Alisa Piekny

Approved by _____
Dr. Selvadurai Dayanandan, Graduate Program Director

January 2015 _____
Dean of Faculty

**ABSTRACT**

## Characterizing Asymmetric Ingression in Mammalian Epithelial Cells

Alexa Mariotti

Cytokinesis occurs at the end of mitosis to divide the cell into two daughter cells. An actomyosin contractile ring forms at the equatorial cortex and ingresses to pinch in the cytosol and membrane. Anillin is a highly conserved protein that binds to components of the ring, mitotic spindle and membrane, and is a key regulator of cytokinesis. The division plane occurs perpendicular to the axis of asymmetry in epithelial cells to ensure that each daughter cell inherits apicobasal polarity. However, these cells undergo dramatic shape changes that involve reorganization of the cytoskeleton during mitosis, and it is not clear how the daughter cells re-establish polarity. Interestingly, contractile ring ingression occurs asymmetricaly in epithelial cells, where one part of the ring appears to move faster and closes near the apical surface. Recent studies using Drosophila epithelial tissue showed that asymmetric ingression occurs due to forces generated near the apical surface of dividing cells, through adhesion with neighbouring cells. We studied cytokinesis in mammalian epithelial cells using Madin Darby Canine Kidney (MDCK) epithelial cells as a model system. Interestingly, we observed that MDCK cells with none or fewer than four neighbours displayed asymmetric ingression, while cells with four or more neighbours were more likely to ingress symmetrically, suggesting that both intrinsic and extrinsic mechanisms influence contractile ring ingression. When induced to form cysts, ingression varied depending on the location of cells within the cyst. The localization of myosin and anillin were uncoupled in asymmetrically dividing MDCK cells, with anillin being more enriched on the ingressing cortex. Anillin may have an important role in asymmetric ingression, since its asymmetric distribution correlated with asymmetric ingression, and its depletion caused cells to ingress more randomly. These results suggest that mammalian epithelial cells possess intrinsic mechanisms for asymmetric ingression, and extrinsic forces applied by neighbouring cells influence their ingression.

**Acknowledgements and Dedications**

I would like to take this opportunity to thank my supervisor, Dr. Alisa Piekny for her continued support, dedication and guidance. Alisa, you believed in me before I believed in myself. Thank you for entrusting me with this novel project and for giving me the chance to pursue my master's degree.

Thank you to my committee members, Dr. Catherine Bachewich and Dr. Christopher Brett for all their valuable advice and expertise.

I would like to give a special thanks to all the members of my lab who have made this experience an unforgettable one. Chloe, thank you for mentoring me during the first few months of my master's degrees and for passing on your invaluable skills. Madhav, thanks for all the support, troubleshooting, and positive vibes. You are truly one of a kind. Denise, your drive, determination and knowledge are contagious. Thank you for rubbing off on me. Tara, thank you for sharing your knowledge, skills and friendship. Melina, your incredible character and knowledge have enriched my experience. Karina, I am so glad to have shared the last year of my masters with you. Your smile, positive attitude and encouragement got me through it all. Danny, there is always something to laugh about when you are bench neighbours with you. Thanks for the months of troubleshooting we went through together.

Finally, all of this would not have been possible without the constant support from my friends and family. Tania, Natasha, Jessica and Erika, thank you for pushing me to be the best that I could be. Who needs siblings when I am so blessed to have you all in my life. Anthony, thank you for sticking by me through it all. You are a key aspect to my success.

I would like to dedicate my thesis to my parents who have supported me through all my various endeavors. Mom, you have been an inspiration to me my whole life. Thank you for teaching me that the road to success is never easy, but going about it alone is not an option. Dad, you have given me the greatest gifts of all: knowledge and laughter. Thank you

for instilling in me your thirst for knowledge and teaching me that after the fact, you can laugh at any situation. Love you both unconditionally.

## Table of Contents

## List of Figures

## Table of Abbreviations

Cdk1 – Cyclin dependent kinase 1

CPC-Chromosome passenger complex

Cyk4-Cytokinesis defect 4 (human MgcRacGAP; Drosophila RacGAP50C)

DAPI-4, 6-diamidino-2-phenylindole

DMEM- Dulbecco's Modified Eagle Medium

DMSO- Dimethyl sulfoxide

Ect2- Epithelial cell transformer sequence 2

FBS-Fetal bovine serum

GEF- Guanine nucleotide exchange factor

GFP-Green fluorescent protein tagged vector

GTP-Guanosine triphosphate

HeLa- Henrietta Lacks cervical cancer cell line

INCENP- Inner centromere protein

MDCK-Madin-Darby canine kidney cells

MLC-Myosin light chain

NDS-Normal donkey serum

Plk1-Polo-like kinase 1

PFA-Paraformaldehyde

RhoA- Ras homolog family, member A

RNAi-RNA interference

TBST- Tris buffer saline (Triton X)

TCA-Trichloroacetic acid

# Chapter 1. Introduction

All cells exhibit some form of polarity in response to their environment, and polarity is essential for cells to give rise to tissues during development (Akhshi, Wernike, and Piekny 2013). Thus, it is crucial for daughter cells to inherit polarity after division, yet it is not known how they can do this when their cytoskeleton undergoes dramatic rearrangements during mitosis. Epithelial tissue is composed of cells that have apicobasal polarity, which continuously divide throughout the lifespan of the organism. The apical surface of these cells face the lumen and are specialized to regulate the movement of molecules. The basolateral surface of these cells contact neighbouring cells as well as the underlying basement membrane. Specialized junctions interconnect cells to ensure that molecules do not freely pass through the epithelial layers, and to tether the actomyosin cytoskeleton across cells for the coordinated transmission of forces (Figure 1). Mutations that disrupt apicobasal polarity or junction formation cause a range of developmental defects and diseases such as polycystic kidney disease, where the kidney tubules accumulate cysts and are unable to properly regulate the removal of waste from the blood (Grant & Kyprianou, 2013).

Madin-Darby canine kidney epithelial cells (MDCK) can be stimulated to form kidney tubules *in vitro,* and are used as a model for studying epithelial cell division. When embedded in a gel mimicking the extracellular matrix (ECM), MDCK cells can form cysts, which are spherical epithelial monolayers formed around a central fluid-filled cavity or lumen. The lumen forms by either hollowing where the membranes separate, or cavitation, when cells in the middle undergo apoptosis (Martin-Belmonte and Mostov 2008; Chung and Andrew 2008; Bryant and Mostov 2008). With the addition of appropriate cues, cysts can develop into tubules closely resembling the functional tubular organs present in the kidneys (Chung and Andrew 2008). Cells within the monolayer can connect with their neighbours via the transmembrane protein E-cadherin, which recruits protein complexes that help establish and maintain apicobasal polarity (Martin-Belmonte and Mostov 2008).

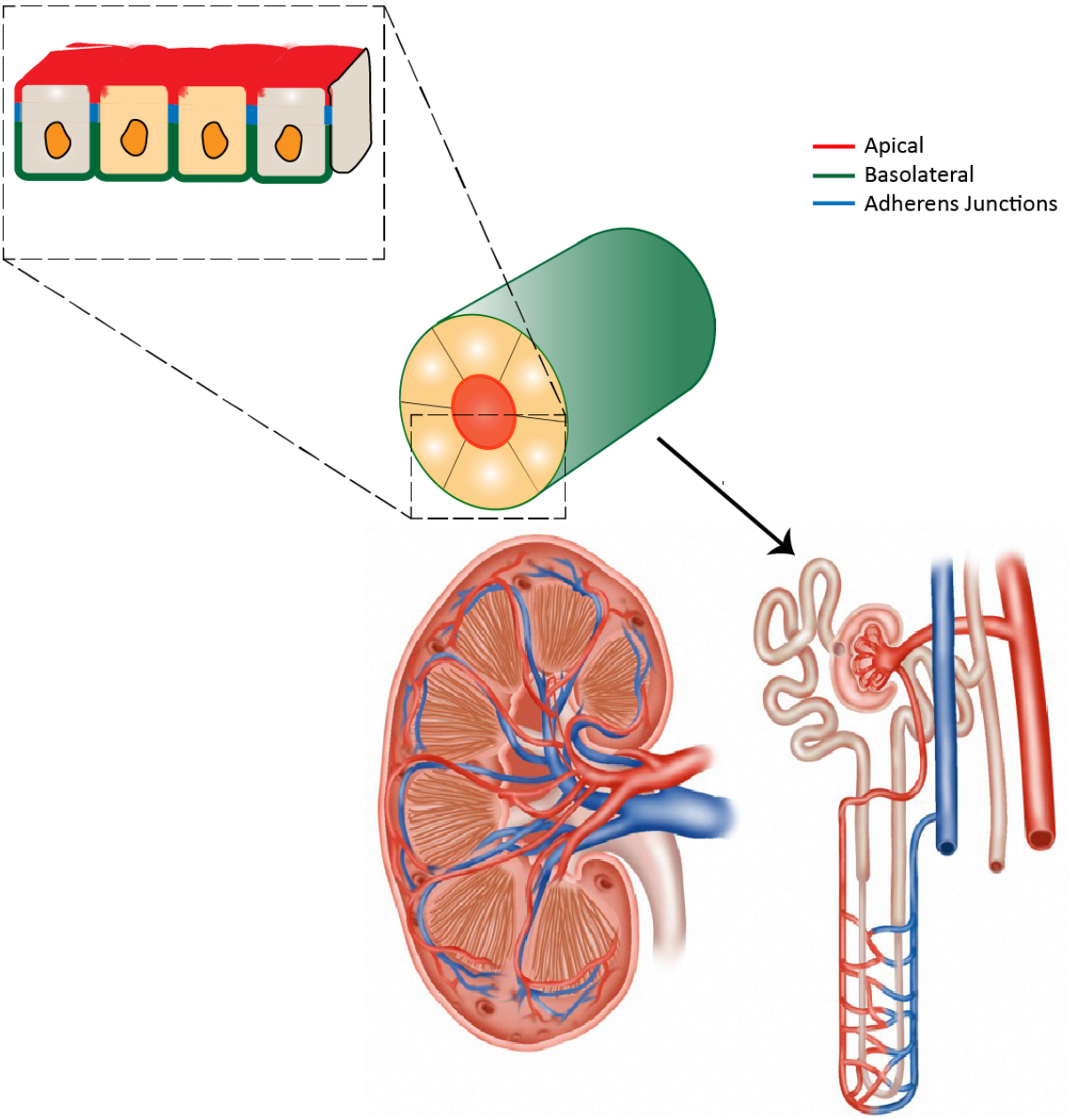


**Figure 1. Organization of epithelial cells, tissues & organs**

A cartoon schematic shows kidney epithelial cells within the epithelial tissue of a kidney tubule, and its location within the kidney. The apical surface (red) faces the lumen, while the basolateral surface (green) contacts neighbouring cells and the underlying basement membrane. Adherens junctions (blue) connect neighbouring cells. *Note: This figure is an*

*adapted figure from* (Ragkousi and Gibson 2014). *Image of the organ was taken from wordpress.com.*

Thus, MDCK cells are a great model system to study how cell division occurs within developing tissues.

We are interested in cytokinesis, the last step in mitosis that physically separates the two daughter cells. Cytokinesis occurs due to the ingression of an actomyosin ring that forms in the equatorial plane of the cell, and is regulated by the small GTPase RhoA (Green, Paluch, and Oegema 2012). During anaphase, Ect2, the GEF (guanine nucleotide exchange factor) for RhoA, is activated by its association with a complex at the mitotic spindle, to generate active RhoA in the equatorial cortex (A. Piekny, Werner, and Glotzer 2005). Active RhoA stimulates the polymerization of F-actin and myosin activation to form and ingress the contractile ring. Active RhoA also recruits the highly conserved scaffolding protein anillin, which binds to actin and myosin, its upstream regulators, microtubules in the mitotic spindle and the overlying membrane, and is considered a key regulator of cytokinesis (Piekny & Maddox, 2010)(Figure 2).

The mitotic spindle provides cues that precisely position the contractile ring to couple it with chromosome segregation. The anaphase spindle has two sets of microtubules: the astral microtubules, which emanate from the centrosomes to the polar cortex, and the central spindle microtubules, composed of bundled, stable, antiparallel microtubules that form between the segregating chromosomes (Hutterer, Glotzer, and Mishima 2009). The astral microtubules exclude the localization of contractile ring proteins at the polar cortex, while the central spindle microtubules direct the accumulation of active RhoA at the equatorial cortex (Akhshi, Wernike, and Piekny 2013; Green, Paluch, and Oegema 2012). Disruption of either set of microtubules causes the localization of contractile proteins to spread along the cortex, while simultaneous disruption of astral and central spindle microtubules causes contractile ring proteins to localize all around the cell cortex (Lewellyn et al. 2010).

The CPC (chromosome passenger complex) regulates cytokinesis and is a multi-subunit complex consisting of INCENP, survivin, borealin and Aurora B kinase. The CPC localizes to the centromeres of kinetochores during metaphase, and the central spindle during

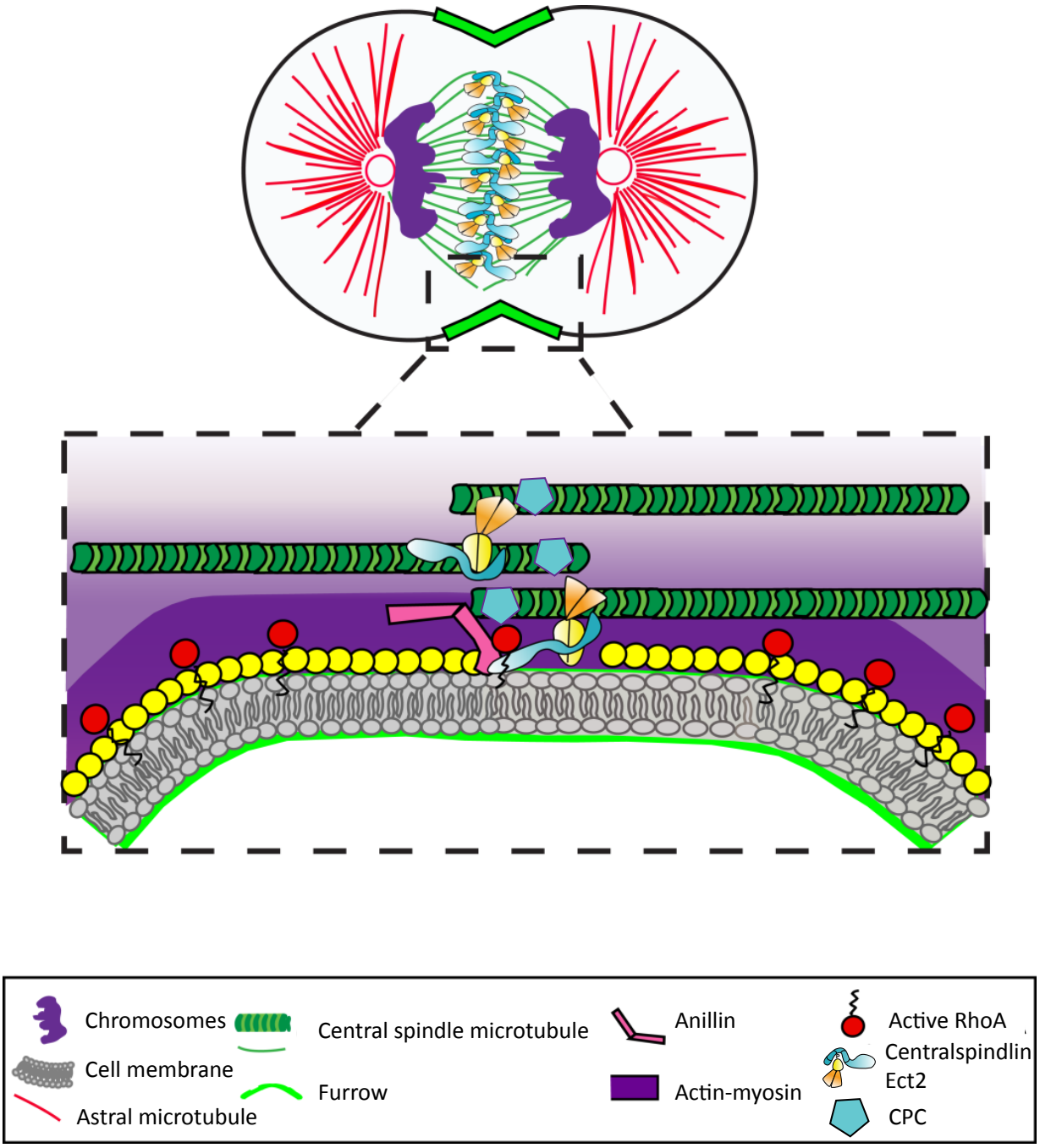


**Figure 2. Schematic of cytokinesis in mammalian cells**

A cartoon schematic shows cytokinesis in a mammalian cell. The central spindle delivers signals for the assembly and ingression of the contractile ring at the equatorial cortex. Centralspindlin recruits Ect2 to generate active RhoA at the overlying cortex. Active RhoA

stimulates F-actin polymerization and myosin activation via effectors, to form and ingress the contractile ring. It also recruits anillin, which binds to actin, myosin, RhoA, the membrane and microtubules to scaffold the ring. *Note: This figure is taken from (Akhshi et al., 2013).*

anaphase, where it regulates the bundling of antiparallel microtubules (Glotzer 2009). Aurora B kinase activity is dependent on its association with the CPC. During anaphase, Aurora B kinase activity forms a gradient around the spindle midzone to act as a spatial organizer of the contractile ring (Fuller 2010). It is not known if Aurora B kinase phosphorylates any cortical proteins, although inhibition of Aurora B blocks the cortical polarization of monopolar cells. After mitotic exit, the levels of Aurora B kinase activity decrease, permitting the cortical re-shaping and spreading of the daughter cells (Floyd et al. 2013).

Epithelial cells are constantly being renewed within organs, yet it is not fully understood how apicobasal polarity is inherited by the daughter cells after division, particularly when their cytoskeletons undergo dramatic reorganization. Interestingly, the mitotic spindle assembles near the apical surface of epithelial cells, which could cause contractile proteins to accumulate differently on the apical vs. basal cortex. The nucleus shifts from its basal position in interphase towards the apical cortex prior to entering mitosis. In both *Drosophila* and zebrafish neuroepithelia, the mitotic nucleus and bulk of the cell cytoplasm are driven apically by actomyosin-dependent cortical contractility that occurs during G2 and prophase (Leung et al. 2011; Meyer, Ikmi, and Gibson 2011). In addition, a microtubule-based mechanism may be involved in nuclear positioning in chicken neural tube cells and in the mouse cerebral cortex, where nuclei migrate apically on microtubules before actomyosin-dependent rounding (Spear, Philip C and Erickson 2012). Cilia-derived centrosomes also migrate from the apical surface on microtubules to meet the nucleus in the centre of the cell. After meeting, the nuclear envelope breaks down and the initial steps of mitotic spindle assembly occur, and shift back toward the apical surface (Peyre et al. 2011; Spear, Philip C and Erickson 2012; Nakajima et al. 2013). Having the mitotic spindle form close to the apical surface of the cell could create gradients of cues that influence the localization of contractile proteins at the apical vs. basal cortex.

Epithelial cells divide parallel to the plane of the epithelium, with the apical surface of the daughter cells remaining in line with the neighbouring cells (Morin and Bellaïche 2011; Tepass 2012; Reinsch 1994). As described earlier, epithelial cells are connected by

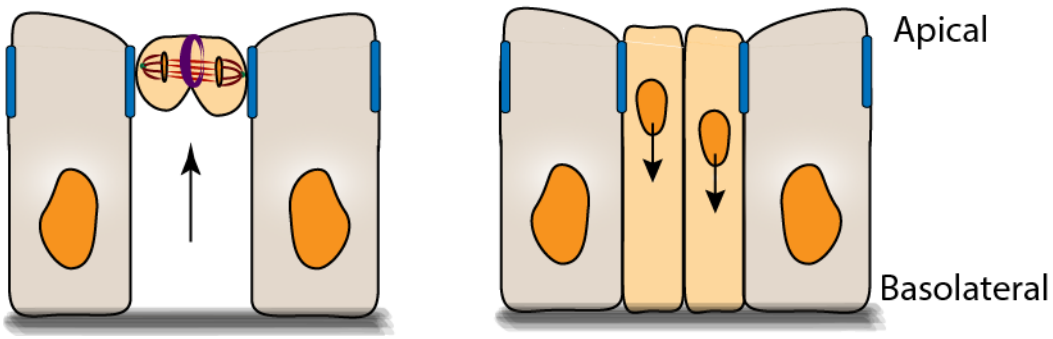


**Figure 3. Schematic of mammalian epithelial cell division**

A cartoon schematic shows epithelial division occurring within the plane of the tissue. Prior to division, the nucleus shifts from its basal position towards the apical cortex, which is coupled with the rounding up of the basolateral cortex during G2. The mitotic spindle assembles near the apical surface, and furrow ingression occurs asymmetrically, from the basal toward the apical side of the cell. After cytokinesis, new junctions form with neighbouring cells and daughter nuclei move basally. *Note: This figure is an adapted figure from (Ragkousi & Gibson 2014)*

adherens junctions, which are composed of E-cadherin, and an intracellular complex of alpha and beta catenin and F-actin. Since the mitotic spindle assembles near the apical surface of cells, as the epithelial cell rounds up, junctions near the basal region are lost, and only subapical junctions are retained. Recent studies in Drosophila epithelial cells suggest that forces generated via junctions near the apical surface cause the contractile ring to ingress asymmetrically, from the basal toward the apical side of the cell (Morais-de-Sá and Sunkel 2013; Guillot and Lecuit 2013)(Figure 3). Having tightly controlled asymmetric ingression could permit the apical surface of the cell to remain distinct from the basal surface, to more easily form well-positioned junctions between the daughter cells (Figure 3).

Here, I investigated cytokinesis in mammalian epithelial cells. I found that MDCK cells with few neighbours undergo asymmetric ingression, while cells with more neighbours ingress symmetrically, suggesting that both intrinsic and extrinsic mechanisms influence the contractile ring. Consistent with this model, cells stimulated to form cysts also displayed either asymmetric or symmetric ingression depending on their location within the cyst. I also found that the localization of myosin and anillin were uncoupled in asymmetrically dividing MDCK cells, with myosin being equally distributed or slightly enriched on the non-ingressing cortex, and anillin being enriched on the ingressing cortex. Anillin may have an important role in asymmetric ingression, since its depletion caused cells to ingress more randomly. These results suggest that MDCK cells possess intrinsic mechanisms for asymmetric ingression, and extrinsic forces applied by neighbouring cells influence their ingression.

# Chapter 2. Material and Methods

## 2.1 Cell Culture and Transfection

MDCK and HeLa cells were grown and maintained in DMEM (Dulbecco's Modified Eagle Medium; Wisent) supplemented with 10% FBS (fetal bovine serum; Thermo Scientific), and PS (100 U penicillin and 0.1 mg/mL streptomycin; Wisent). HeLa cells required an additional supplement of 2 mM L-glutamine. Cells were grown in a humidified incubator with 5% $CO_2$ at 37°C. For maintenance, stock plates were grown to a confluency of 80-90%, then split by washing cells with pre-warmed PBS (phosphate buffered saline; Wisent), then adding 400 µL of 0.25% trypsin and incubating the cells at 37°C for 5 minutes. The cells were observed under an inverted light microscope to ensure that they had fully detached prior to resuspending them in 10 mL of pre-warmed DMEM with FBS and PS. After pipetting up and down vigorously, drops of cells were added to a new culture dish with 10 mL of pre-warmed DMEM with FBS and PS. Cells were passaged a maximum of 22 times prior to thawing a fresh stock. For transfection, cells were grown on 25 mm glass coverslips (No. 1.5; Harvard Apparatus) in DMEM with FBS, but without antibiotics (PS-free), until they reached a confluency of 50-60%. Before use, coverslips were washed with 0.1 M HCl, then with isopropanol, after which they were air-dried in 6-well plates. DNA transfections were performed using Lipofectamine (Invitrogen) according to manufacturer's protocol, except that 3-6 µL of reagent was used per 2 mL of media to limit lethality. For optimal transfection, the amount of DNA used varied for each cell construct (e.g. 1 µg for H2B:mRuby, 3 µg for full-length GFP:anillin and 1.5 µg for c-term GFP:anilllin). For live imaging, coverslips were used 24-26 hours after transfection. Co-transfection of DNA and siRNAs (4 µL of 2.0 nM siRNAs) was performed using Lipofectamine as outlined above, and cells were imaged 22-27 hours after transfection. Transfection of siRNAs were performed using Oligofectamine (Invitrogen) according to manufacturer's instructions (except that 9-12 µL of Oligofectamine was used per 2 mL of media). For optimal RNAi transfection, cells were transfected at ~40-50% confluency, and the media was removed prior to adding the siRNA mixture for 4-5 hours. The mixture was then replaced with DMEM with FBS (PS-free), and cells were left for an additional 25-30 hours before fixing or

performing live imaging.

### 2.2 RNAi and Drug Treatments

The following siRNA sequence was used to target the anillin gene as previously described: 5' CAUAUAAGUCUAAGGAAU 3' (Thermo Scientific). To inhibit Aurora B kinase, 1 μM of ZM447439 (Abmole Bioscience) was added to cells for 20-40 minutes prior to their fixation. ZM447439 was dissolved in DMSO as a 1000X stock and stored at -20°C.

### 2.3 Cell Lines

MDCK cell lines expressing mCherry:tubulin and GFP:MLC (active) were generated by G418 antibiotic (Wisent) selection followed by dilution cloning. MDCK cells were transfected as described in Chapter 2.1. After 24 hours, cells were washed with 1 X PBS followed by the addition of pre-warmed DMEM with FBS. 100 μL of G418 (100 mg/mL) was added to the media to kill non-expressing cells. The cells that survived were trypsinized (400 μL 1X trypsin; Wisent) and diluted by a factor of 10,000 into 10 cm plates containing pre-warmed DMEM media with FBS. The diluted cells were grown for 24-48 hours with G418 (50 μL). The positive clones were screened by fluorescent microscopy and isolated from the surrounding cells using a homemade plastic ring coated in petroleum jelly that matched the size of the clone of interest, which was placed on the plate after removing the media. Cells within the clone were trypsinized by adding a drop of trypsin inside the ring. After 60 seconds, the cells from one clone were transferred to one well of a 12-well dish containing 1 mL of fresh DMEM media with 10% FBS. Cells were grown for another 24-48 hours in the presence of 50 μL of G418, then checked for viability and fluorescence. If the clones were more than 70% fluorescent, then the cells were transferred to a 6-well dish, then grown to confluency followed by another transfer to a 10 cm dish prior to freezing. If the fluorescent levels were lower than 70%, then additional screening was performed. To freeze cells, they were trypsinized from the 10 cm dish, then centrifuged for 5 min at 1,000 rpm after resuspending cells in DMEM with FBS. After pelleting, the media was aspirated and cells were resuspended in 2 mL of freezing media (10% DMSO, 50% FBS and 40% DMEM). Afterwards, 1 mL of the cell suspension was added to a tube suitable for cryostorage, and placed in a specialized freezing containers with a cooling rate of -1 °C/min

(Mr. Frosty freezing container, Thermo Scientific) then placed at -80 °C. After reaching -80 °C (or within ~2 weeks), they were transferred to liquid nitrogen for long-term storage. Tubes were labeled according to perceived expression levels; *e.g.* weak vs. strong fluorescence.

**2.4 Fixing and Immunofluorescence**

To fix cells for immunostaining, they were washed with pre-warmed 37°C cytoskeletal buffer (80 mM PIPES, 1 mM MgCl2, 5 mM EGTA), then incubated in either 100% cold MeOH (stored at -20°C) for 20 minutes (to stain for anillin, tubulin, myosin, Aurora B), 10% w/v cold trichloroacetic acid (100% TCA prepared 30-60 minutes in advance) for 15 minutes (to stain for anillin and E-cadherin), or 4% w/v paraformaldehyde at room temperature for 20 minutes (to stain for GFP and E-cadherin). After fixing, the cells were washed 3-4 times with 1X TBST buffer (0.5% Triton X-100, 0.15 M NaCl and 0.05 M Tris, pH 7.0), then the coverslips were placed in a wet chamber (a covered plastic dish with wet paper towels to prevent drying) and cells were blocked with 5% NDS (Normal Donkey Serum) and TBST for 20 minutes. Cells were then immunostained by incubating them with primary antibodies for 2 hours at room temperature using the following dilutions in TBST with 5% NDS: 1:200 rabbit anti-anillin antibodies (A. J. Piekny and Glotzer 2008), 1:200 mouse anti-tubulin antibodies (DM1A, Sigma-Aldrich), 1:100 rabbit anti-nonmuscle myosin II (Sigma-Aldrich), 1:100 mouse anti-Aurora B (BD Transduction Laboratories), 1:50 mouse anti-GP135 (Developmental Studies Hybridoma Bank), mouse 1:100 anti-E-Cadherin (BD Transduction Laboratories) and 1:200 rabbit anti-GFP antibodies a gift from Michael Glotzer (University of Chicago). The cells were subsequently washed 3 times with TBST, then incubated with secondary antibodies for 2 hours at room temperature using 1:250 dilutions in TBST with 5% NDS of anti-mouse or anti-rabbit Alexa 488, with anti-rabbit or anti-mouse Alexa 568 (Invitrogen). Cells were then washed 2 times with TBST prior to adding 1:000 DAPI (4, 6-diamidino-2-phenylindole; 1 mg/mL; Sigma-Aldrich) in TBST for 5 minutes. Cells were washed again with TBST before a final wash with 0.1 M Tris pH 8.8. After aspirating remaining liquid, a drop of mounting media (4% n-propyl gallate in 50% glycerol, 0.1 M Tris pH 8.8) was added to the coverslip, which was then mounted onto a glass slide. Excess liquid was absorbed using a Kimwipe (Kimtech) then sealed with nail

polish.

**2.5 Microscopy**

Fixed cells were imaged using the Leica DMI6000B inverted microscope (Leica Microsystems) with the 40X/0.75 NA or 63X/1.4 NA oil immersion objectives and the Hamamatsu digital CCD ORCA R2 camera with Volocity acquisition software (PerkinElmer). Z stacks of 0.5 μm thickness were acquired using the piezo Z stage (Mad City Labs). The exposure times were set according to control slides and kept below 4000 levels. Fixed cysts were imaged using the Olympus Fluoview FV10i confocal laser scanning microscope (Olympus) with the 10X/0.4 NA air objective or 60X/1.35 NA oil immersion objective. Images were taken with a resolution of 1024 X 1024 pixels, with the aperture at 1.5. Z sections of 0.3 μm thickness were collected. Images were opened in Image J (NIH) and maximum intensity z-stack projections were generated for further analysis.

To perform live imaging, cells grown on 25 mm round coverslips were placed in a 35 mm Chamlide magnetic chamber (Quorum) with pre-warmed DMEM with FBS. Cells were kept at 37°C with 5% $CO_2$ using the INU-TiZ-F1 stage series chamber. Live imaging was performed on an inverted Nikon Eclipse Ti microscope with a Livescan Swept Field confocal unit (Nikon), the 60X/1.4 NA oil immersion objective, and the iXON897 EMCCD camera (Andor) using Elements acquisition software (Nikon). A slit size of 50 μm was used with the 488 and 561 nm lasers set between 20-60% (100 mW, Agilent). Z-stacks of 0.5 μm were collected using the piezo Z stage Nano-Z100 N (Mad City Labs) every 40 to 60 seconds. Live imaging also was performed on an inverted Nikon Ti epifluorescent microscope using the 60X/1.4 oil immersion objective, and an Evolve (EMCCD, 512X512) camera with Elements 4.0 acquisition software (Nikon). Images were acquired using the 488 and 561 filters and the Heliophor LED source (National Instruments), and z-stacks of 0.2 μm thickness were collected using the NI-DAQ piezo Z stage (National Instruments) every 30 seconds. Movies were opened in Image J and maximum intensity z-stack projections were generated.

GFP:MLC movies were imported into Autoquant X software (Media Cybernetics) for deconvolution using a point spread function (PFS) customized for the microscope. After

deconvolution, the images were opened in IMARIS software (Bitplane) where 3D-surface projections were created and saved as snapshot TIFF images or AVI movie files.

### 2.6 Measurements

All measurements were performed on z-stack maximum intensity projections in Image J. The breadth of accumulated protein was calculated by performing line scans along each cortex of the cell, then counting the number of pixels above 50% of the maximum pixel intensity. The number of pixels was converted to distance in μm (depends on the objective) in Excel (Microsoft), and the breadth to length ratio was determined by dividing the breadth by the total length of the linescan. Standard deviations and averages were also calculated in Excel (Microsoft), which were then plotted onto graphs. The total amount of protein at each cortex was determined by summing the intensity values along the linescan. The velocity of furrow ingression was calculated by measuring the distance that each cortex moved from the start of furrow ingression to the end, divided by the time. Velocities were measured during early (1/3$^{rd}$ ingression), mid (1/2 ingression) and late ingression (2/3$^{rd}$ ingression). The threshold for asymmetry was determined by comparing the distance for each cortex from the future midbody site (end of ingression). If the ratio of the cortices was higher than 1.2 or less than 0.8, then the cell was classified as asymmetric.

### 2.7 Cysts

To generate MDCK-cell derived cysts, cells were added to a chamber with matrigel to create a 3D environment for stimulating tissue formation. To make the matrigel chambers, a 4-well chamber slide system 154526 (Lab-Tek II) was left to cool on ice for 15 minutes prior to adding 40 μL of 100% matrigel (BD Bioscience) to each well. The matrigel was spread using a pipette tip to all 4 corners of the wells and left to cool for 1 minute before excess reagent was removed. This procedure was repeated twice. Next, the coated chamber slide was left to polymerize; 15 minutes on ice (~0°C), 15 minutes at room temperature (~22°C) followed by 1 hour in a humidified incubator with 5% $CO_2$ at 37°C. As the chamber slide was being made, MDCK cells were trypsinized for 10-12 minutes at 37°C followed by their resuspension in 2 mL of DMEM media with 10% FBS. Then, 1 mL of the resuspended cells was added to a 15 mL polypropylene tube and centrifuged for 5 minutes

at 1,000 rpm. The supernatant was removed by aspiration and the pellet was resuspended in 1 mL of fresh DMEM media with FBS. The hematocytometer was then used to calculate the dilution needed to obtain cells at a final concentration of 2.0 X $10^4$ – 5.0 X $10^4$ by adding 40 µL of resuspended non-diluted cells and counting the 4 outer most squares under the microscope, then calculating the concentration using the formula:

Total cells/mL: Total cells counted * (dilution factor/# of squares counted) * 10000 cell/mL

With this final concentration in mind, cells were mixed with 2% matrigel to obtain a total volume of 600 µL, which was added to the coated chamber slide. Cells were left to develop into cysts for 3 to 5 days. 400 µL of fresh DMEM media with FBS was added to the chamber every 3 days.

**2.8 Fixing and Immunofluorescence of Cysts**

Prior to fixing, each chamber containing grown cysts embedded in matrigel were rinsed 3 times with 200 µL of 1 X PBS pH 7.4. Residual PBS was removed with a pipette, and not by aspiration to not disturb the matrigel. Cysts embedded within the matrigel were fixed at room temperature by adding 200 µL of freshly made 4% w/v paraformaldehyde in 1X PBS at pH 7.0 for 30-40 minutes. Then, the fixed cysts were washed 3 times for 5 minutes each with 1 X PBS after which 200 µL of 0.5% Triton X-100, 0.1% BSA, 5% NDS in 1 X PBS was added per well to permeabilize and block the cysts for one hour at room temperature. The cysts were then incubated with primary antibodies diluted in 1 X PBS with 5% NDS overnight at 4°C, with the following dilutions: 1:50 mouse anti-GP135, mouse 1:100 anti-E-Cadherin and 1:200 rabbit anti-GFP (gift from Michael Glotzer, University of Chicago). After, the cysts were washed 3 times for 5 minutes each using 0.5% Triton X-100, 0.1% BSA in 1 X PBS. Next, the cysts were incubated with the following secondary antibodies for 2 hours at room temperature, diluted 1:250 in 1 X PBS with 5% NDS: anti-rabbit Alexa 488 and anti-mouse Alexa 568 (Invitrogen). The cysts were then washed 2 times using 1 X PBS, then 1:000 DAPI (4, 6-diamidino-2-phenylindole; 1 mg/mL; Sigma-Aldrich) was added for 5 minutes prior to washing cells 3 times for 5 minutes each with 1 X

PBS. Finally, the cysts were washed once with 0.1 M Tris pH 8.8, then a drop of mounting media (4% n-propyl gallate in 50% glycerol, 0.1 M Tris pH 8.8) was added to the slide, after which a coverslip was added and sealed with nail polish.

## Chapter 3. Results

The main goal of my studies was to characterize cytokinesis in mammalian epithelial cells using MDCK cells as a model system. These cells have different properties compared to other cultured mammalian cells classically used to study cytokinesis, such as Hela cells. We wanted to determine if these properties impart any changes on the cytokinetic machinery. For example, MDCK cells express E-cadherin that forms homotypic adhesion with other E-cadherin-expressing cells (Chung and Andrew 2008). The forces imparted by adhesion with other cells could influence forces associated with furrow ingression. Although it is ideal to study these cells within the context of a developing tissue, MDCK cells grown as a monolayer still display accumulation of E-cadherin at cortices adjacent to neighbouring cells suggesting that they can adhere to one another. While these cells may not display true apicobasal polarity, the forces generated from this adhesion could still shed light on how the constraints of neighbouring cells influences cytokinesis of cells within tissues.

### 3.1 MDCK cells have asymmetric ingression

We hypothesized that MDCK cells in monolayers may undergo cytokinesis differently in comparison to previously studied cell types, such as Hela cells, because they would be susceptible to forces generated by adhesion with neighbouring cells. In support of this hypothesis, we examined populations of cells in monolayers and found that a large number of cells had asymmetric ingression, with one cortex moving over a larger distance vs. the other cortex (Figure 4A). Cells were deemed asymmetric if the ratio of the distances for the two cortices deviated from 1 (e.g. >1.2 or < 0.8; *e.g.* Figure 5C). We examined fixed cells grown at two different confluencies: at low confluency where there were a greater number of cells with few neighbours, and at high confluency where cells were more likely to be surrounded by neighbours (Figure 4C). A greater proportion of cells at low confluency had asymmetric ingression (89.5% +/- 20.3%, n=20) vs. cells at high confluency (50% +/- 13.2%, n=20). Interestingly, cells with 4 or less neighbours displayed asymmetric

**A.**

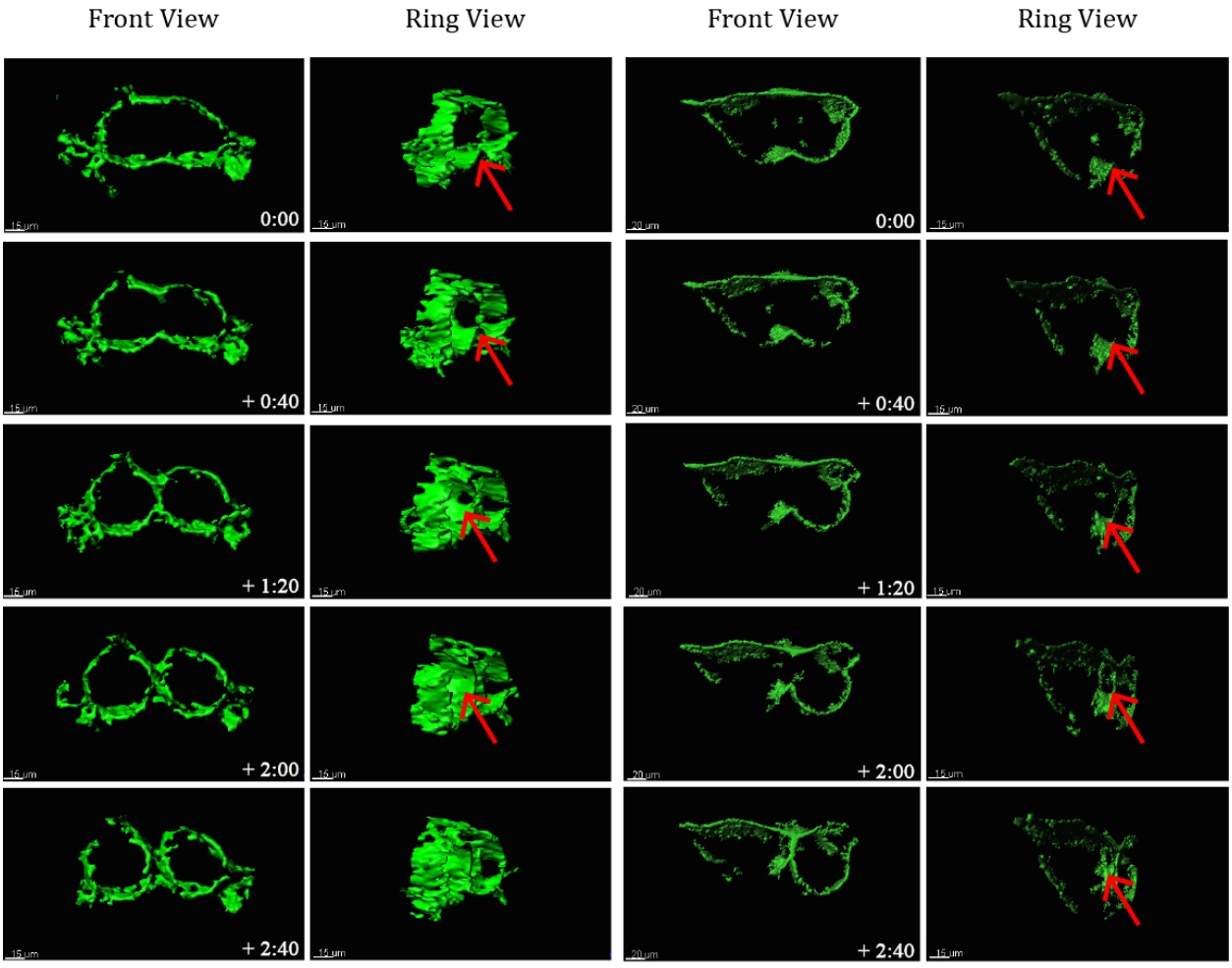
Front View
Ring View
Front View
Ring View
0:00
+ 0:40
+ 1:20
+ 2:00
+ 2:40
0:00
+ 0:40
+ 1:20
+ 2:00
+ 2:40
Symmetric Ingression
Asymmetric Ingression

**B.**

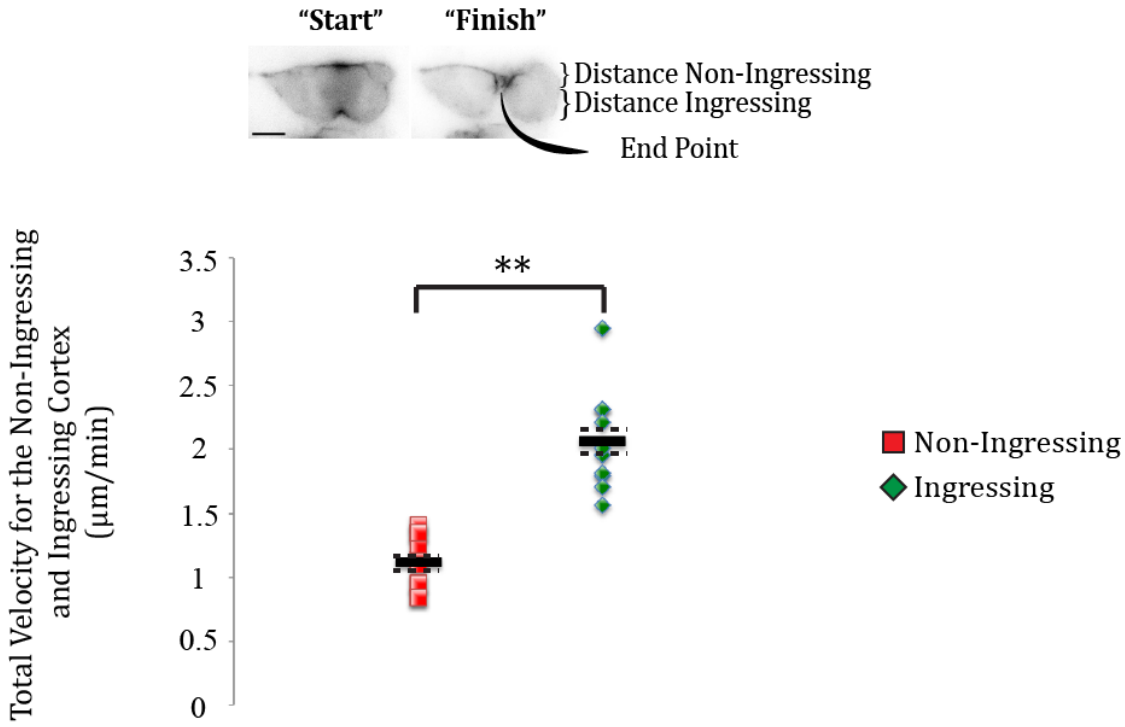
"Start"
"Finish"
} Distance Non-Ingressing
} Distance Ingressing
End Point
Total Velocity for the Non-Ingressing and Ingressing Cortex (µm/min)
3.5
3
2.5
2
1.5
1
0.5
0
**
Non-Ingressing
Ingressing

**C.**

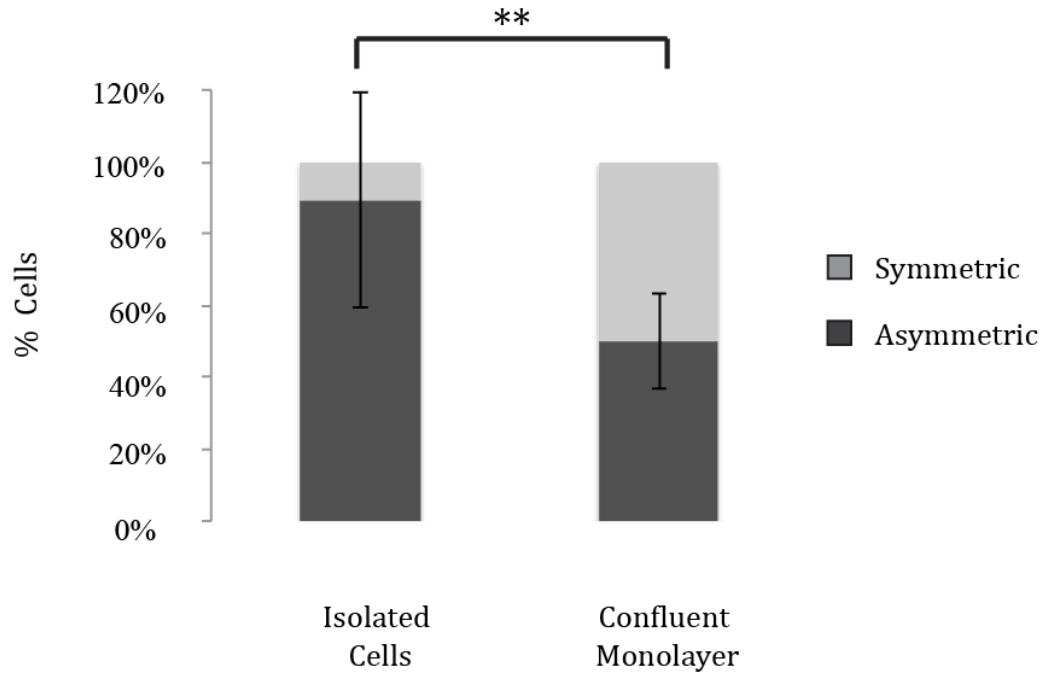
**
120%
100%
80%
60%
40%
20%
0%
% Cells
Symmetric
Asymmetric
Isolated Cells
Confluent Monolayer

**D.**

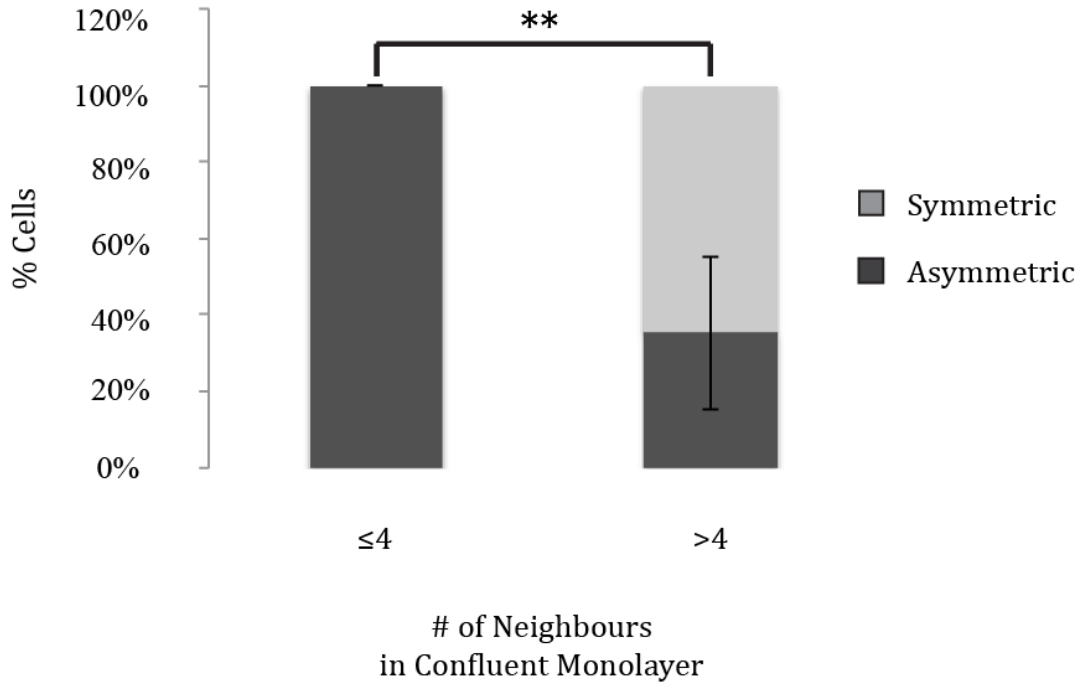


**Figure 4. MDCK cells ingress asymmetrically, which is dependent on the number of neighbouring cells.**

A) Live imaging of an MDCK cell stably expressing GFP-tagged active myosin during ingression. Movies were deconvolved and surface rendered to best see the asymmetric ingression and ring closure for symmetric and asymmetric cells. Red arrows point to the contractile ring as it ingresses. B) The start and finish time points show how the ingression distances were calculated for each cortex. The graph shows the velocities of each non-ingressing (red) and ingressing cortex (green; n=10). C) A bar graph shows the proportion of cells that ingress symmetrically or asymmetrically when they are isolated, or in a confluent monolayer (n=20 for each set). D) A bar graph shows the proportion of cells that ingress symmetrically or asymmetrically based on the number of neighbours they have when grown in a confluent monolayer (n=20). For both graphs, the black bars show standard deviation, and ** is $p < 0.01$ based on the student's t test.

ingression (100% +/- 0%; n=20), while cells surrounded by more than 4 neighbours were more likely to display symmetric ingression (64.7% +/- 20%, n=20; Figure 4D). This suggests that neighbouring cells impart forces on the dividing cell, but when there are fewer (or no neighbours), there is an intrinsic system that is already asymmetric and the external forces can override this system if there are too many neighbouring cells. To further characterize asymmetric ingression, we performed live imaging of MDCK cells stably expressing GFP-tagged active myosin light chain (GFP-MLC) from anaphase to the end of telophase (Figure 4A,B, 5A). As expected, I saw two groups of cells. One group of cells ingressed symmetrically, similar to Hela cells (18.9 +/- 19.9%), while the second group displayed asymmetric ingression (81.1+/- 19.9%; 20<n<50). I determined the ingression rate of each cortex in asymmetric cells from the start of ingression until both cortices met, by measuring the total distance travelled by each cortex over time (Figure 4B, 5B). Indeed, I found that one of the cortices (with no neighbours) ingressed much faster in comparison to the other cortex (which had neighbours). I performed similar measurements on Hela cells for comparison, and found that while the ratio of the non-ingressing cortex to the ingressing cortex was 0.5 for MDCK cells, both cortices ingressed similarly in Hela cells with a ratio close to 1 (0.8; Figure 5C). These results suggest that MDCK cells undergo cytokinesis differently vs. Hela cells, and their adhesion with neighbouring cells influence cortical ingression.

### 3.2 Active non-muscle myosin is evenly distributed in MDCK cells

Since furrow ingression is mediated by myosin contractility, we wanted to determine if the asymmetric furrow ingression we observed in MDCK cells occurs as a result of the unequal recruitment of active myosin to the division plane. We characterized myosin localization by imaging asymmetrically ingressing MDCK cells stably expressing GFP-tagged active myosin light chain (GFP-MLC) during cytokinesis. Myosin was enriched in the equatorial plane, similar to Hela cells, but appeared to be slightly enriched and broader along the non-ingressing cortex (Figure 6A). To measure this, we quantitated the ratio of the breadth of myosin accumulation along each cortex vs. cell length during

**A.**

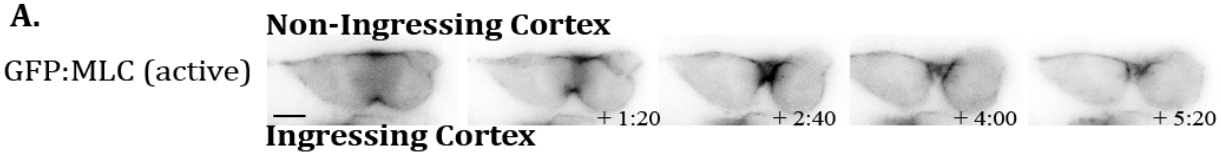
GFP:MLC (active)
Non-Ingressing Cortex
+ 1:20
+ 2:40
+ 4:00
+ 5:20
Ingressing Cortex

**B.**

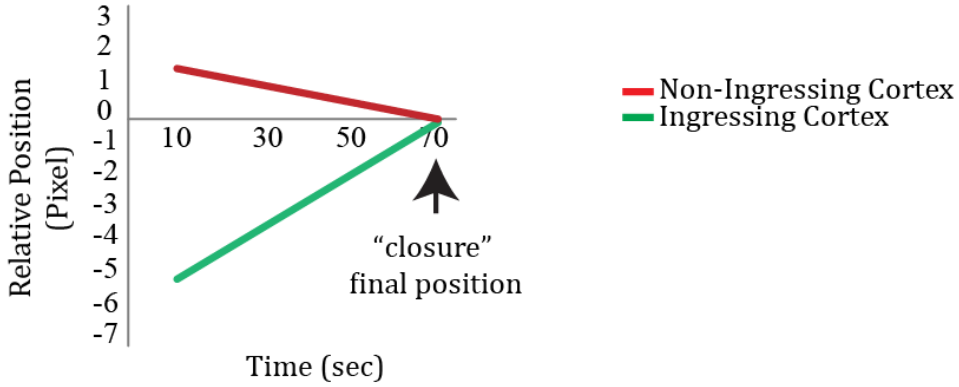
Relative Position (Pixel)
3
2
1
0
-1
-2
-3
-4
-5
-6
-7
10
30
50
70
"closure" final position
Time (sec)
Non-Ingressing Cortex
Ingressing Cortex

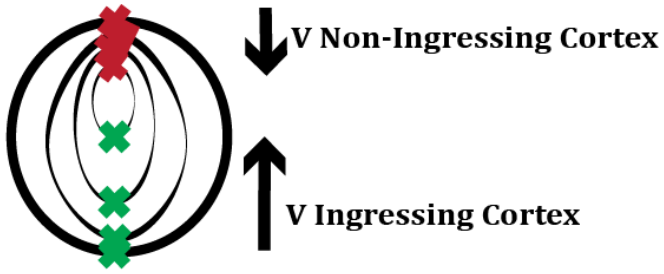
V Non-Ingressing Cortex
V Ingressing Cortex

**C.**

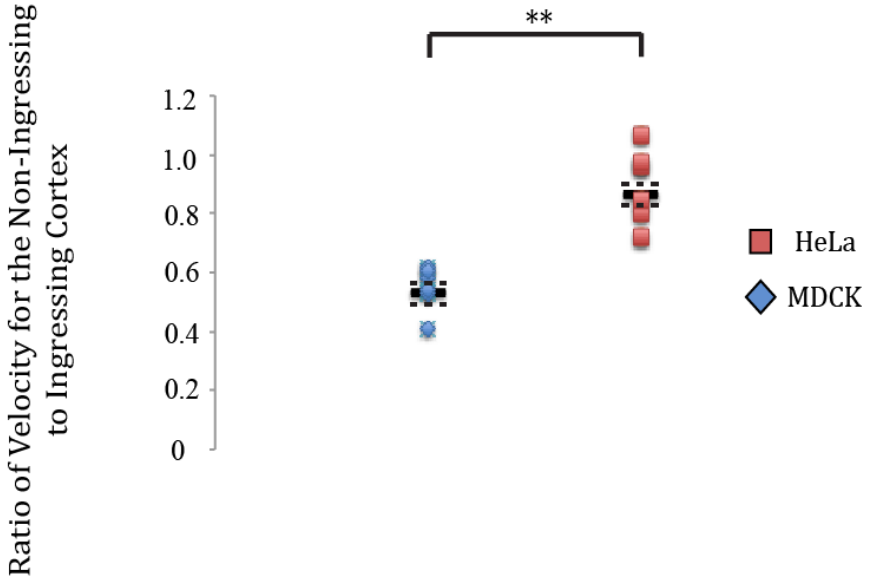
Ratio of Velocity for the Non-Ingressing to Ingressing Cortex
**
1.2
1.0
0.8
0.6
0.4
0.2
0
HeLa
MDCK

### Figure 5. MDCK cells ingress asymmetrically in comparison to Hela cells

A) Images are shown from an MDCK cell stably expressing GFP-tagged active myosin during cytokinesis. B) The relative positions of the non-ingressing and ingressing cortex during furrow ingression are shown over time. C) The graph shows the velocity ratio for the non-ingressing vs. ingressing cortices in HeLa cells (red) and MDCK cells (blue). For all graphs, the solid black bars show the average, while the dotted bars show the standard deviation, and ** is $p < 0.01$ based on the student's t test. The scale bar is 10 μm.

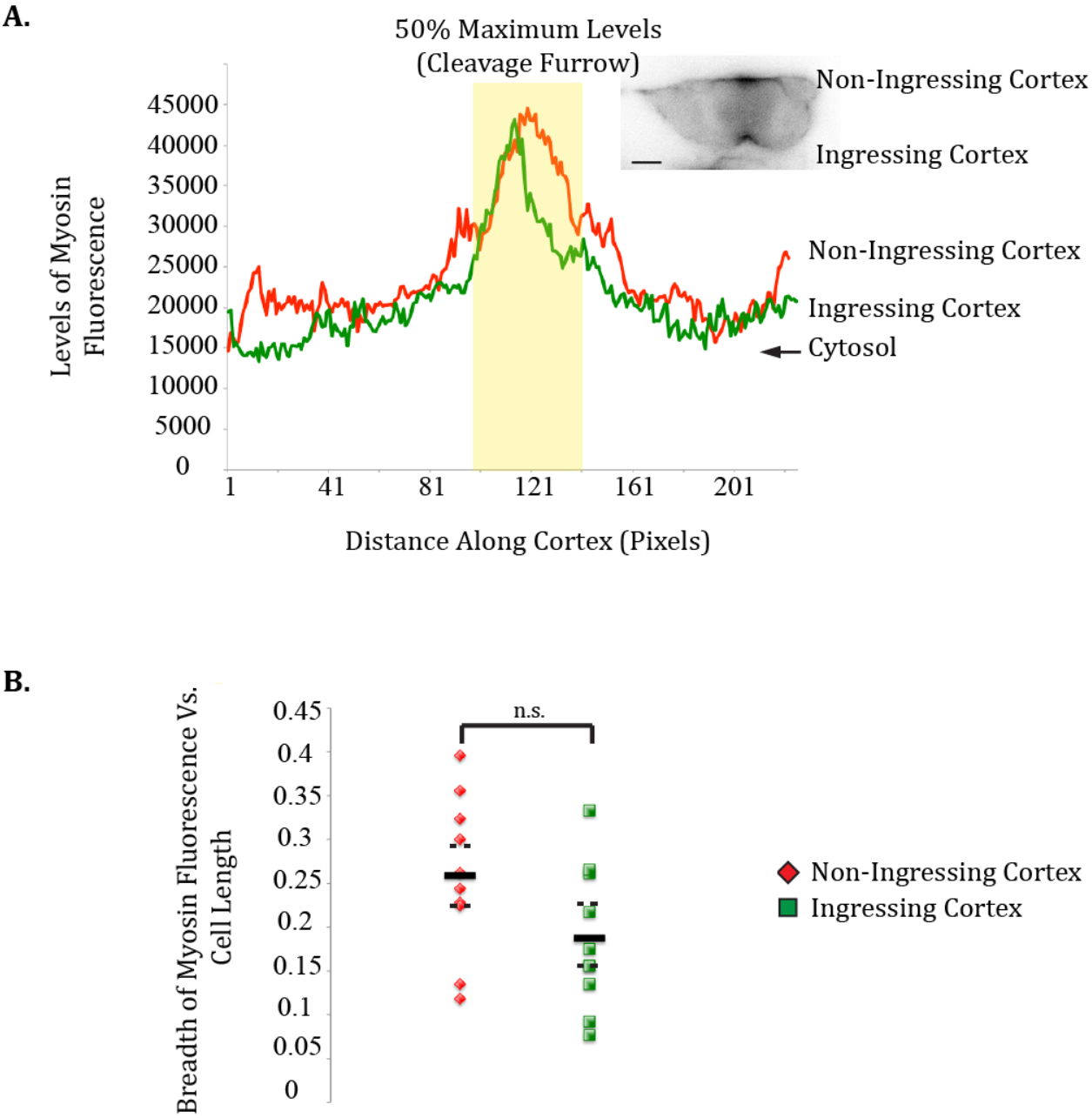


**Figure 6. Active non-muscle myosin is evenly distributed in asymmetrically ingressing MDCK cells**

A) A graph shows line scans of GFP-tagged active myosin along the non-ingressing (red) and ingressing (green) cortices of an MDCK cell. The breadth of myosin along each cortex is highlighted by the yellow box, which was measured as the number of pixels above 50% of the maximum levels. B) A graph shows the ratio of breadth of myosin vs. cell length on the

non-ingressing (red) and ingressing cortex (green) for multiple cells (n=10). The solid black bars represent the average, while the dotted bars represent the standard deviations for each data set. The student t test was used to test for significance. The scale bar is 10 μm.

ingression. The breadth was determined as the number of pixels above half the maximum intensity of GFP by line scans drawn along each cortex and the ratio was calculated by dividing the breadth by the total number of pixels for each cortex (Figure 6A). My results showed that the average ratio of myosin accumulation vs. cell length was 0.25 +/- 0.08 on the non-ingressing cortex and 0.18 +/- 0.08 on the ingressing cortex (Figure 6B). Therefore, myosin distribution does not explain the difference in ingression rates for the two cortices, since we would have expected the ingressing cortex to have more active myosin vs. the non-ingressing cortex.

### 3.3 Anillin's basal enrichment correlates with asymmetric ingression in MDCK cells

Even though the localization of active myosin is not dramatically altered in MDCK cells, other regulators of the contractile ring could be distributed differently around the cortex to drive asymmetric ingression. One of these proteins is anillin, which binds to both F-actin and active myosin as described in Chapter 1. To characterize the accumulation of anillin in MDCK cells during ingression, we performed live imaging of cells transiently expressing GFP-tagged full-length anillin, and calculated the ratio of breadth to length along each cortex as described above (Figure 7A,B). Interestingly, in symmetrically ingressing cells, the ratio of the breadth of anillin to cell length was similar for each cortex (mid-ingression: 0.15 +/- 0.06 vs. 0.15 +/- 0.05; late-ingression: 0.09 +/- 0.03 vs. 0.08 +/- 0.03), while in cells ingressing asymmetrically, the ratio was very different for each cortex (mid-ingression: non-ingressing 0.12 +/- 0.03 vs. ingressing 0.29 +/- 0.10; late-ingression: non-ingressing 0.07 +/- 0.04 vs. ingressing 0.44 +/- 0.09, $10<n<20$; Figure 7C). We also measured anillin breadth vs. cell length in Hela cells for comparison, and found that as expected, the ratio was similar for each cortex (Figure 7D). The correlation between asymmetric anillin localization and asymmetric furrow ingression in MDCK cells suggests that anillin could be important for this process. However, it is not clear how anillin could promote asymmetric furrowing. As described earlier, we found that cells with 4 or less neighbours were more likely to ingress asymmetrically, and we observed that the cortex that ingressed asymmetrically was the side of the cell that was 'free' from neighbours.

**A.**

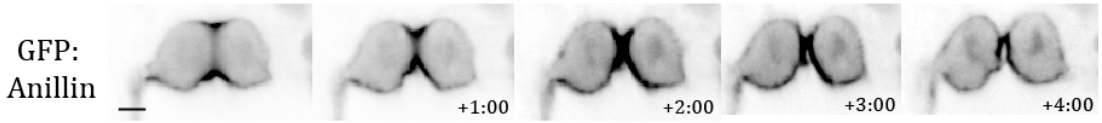
GFP:
Anillin
+1:00
+2:00
+3:00
+4:00

**B.**

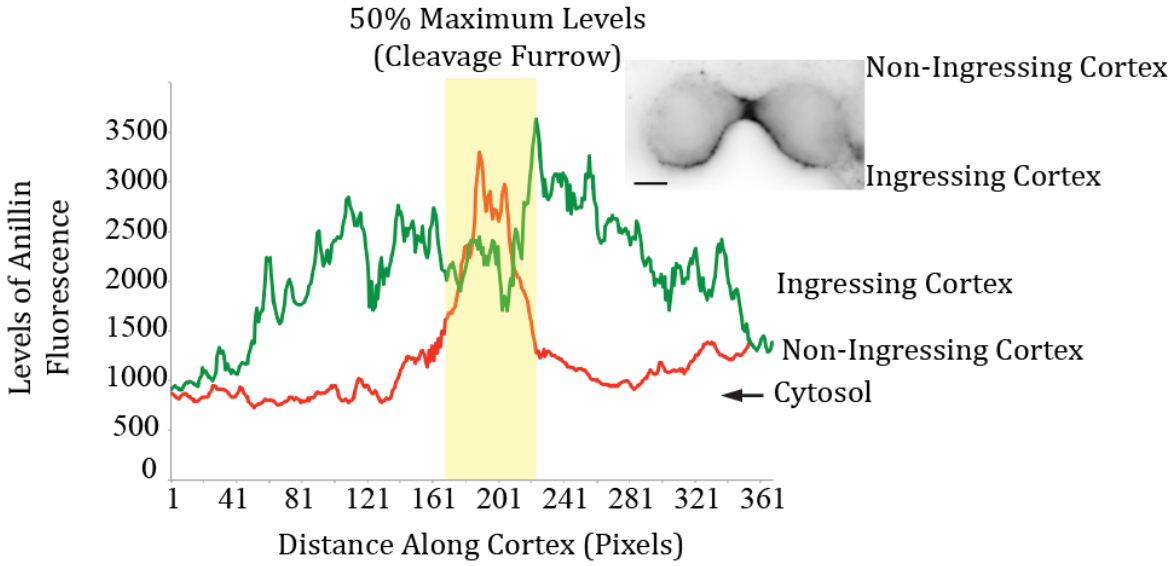
50% Maximum Levels
(Cleavage Furrow)
Non-Ingressing Cortex
Ingressing Cortex
Ingressing Cortex
Non-Ingressing Cortex
Cytosol
Levels of Anillin Fluorescence
3500
3000
2500
2000
1500
1000
500
0
1
41
81
121
161
201
241
281
321
361
Distance Along Cortex (Pixels)

**C.**

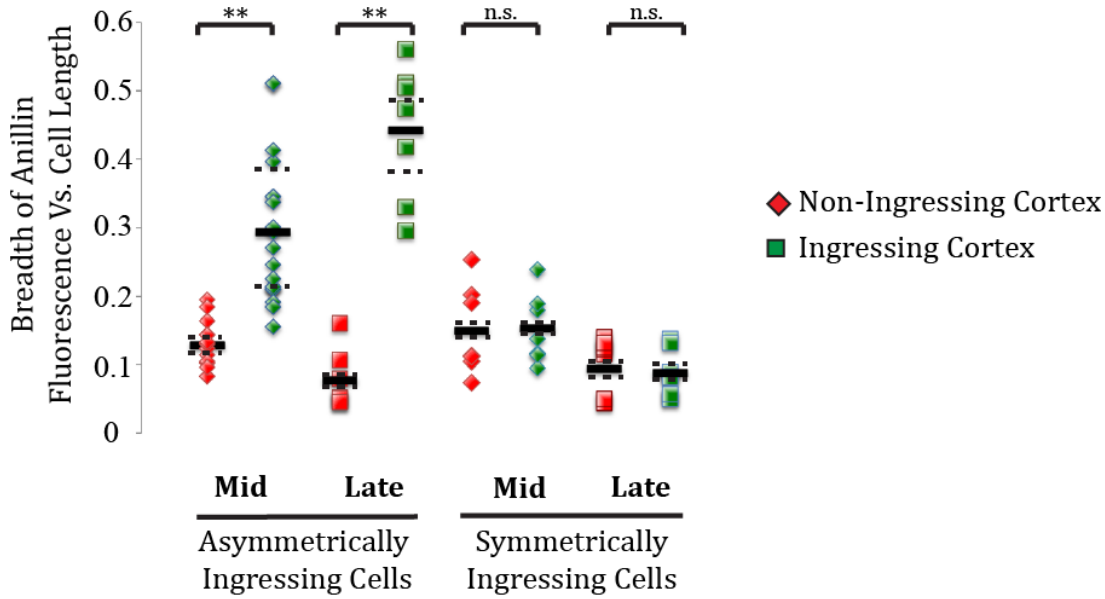
Breadth of Anillin Fluorescence Vs. Cell Length
0.6
0.5
0.4
0.3
0.2
0.1
0
**
**
n.s.
n.s.
Mid
Late
Mid
Late
Asymmetrically Ingressing Cells
Symmetrically Ingressing Cells
Non-Ingressing Cortex
Ingressing Cortex

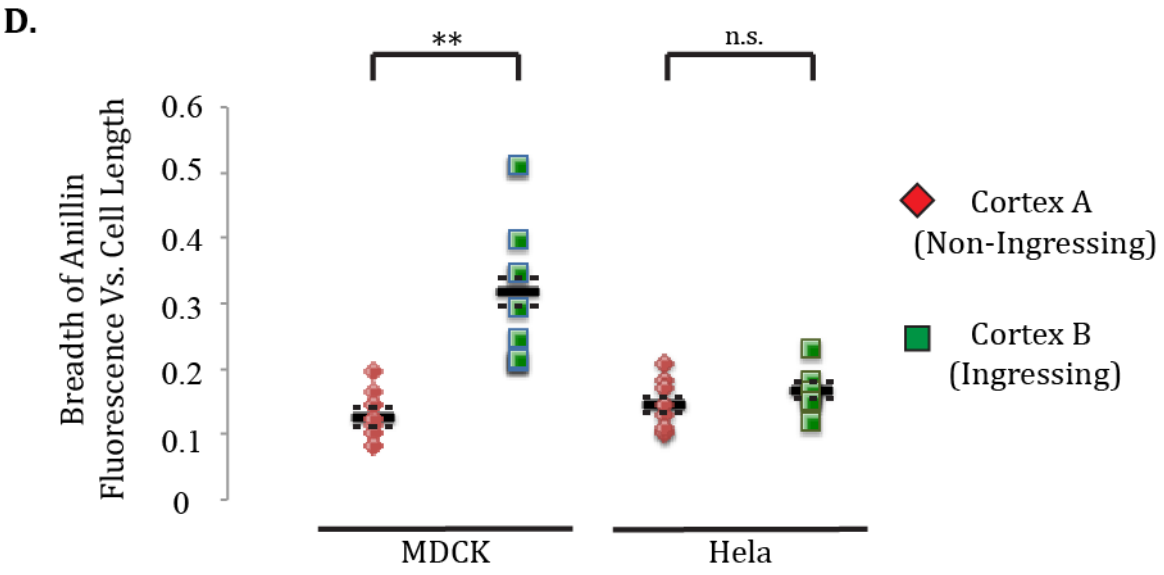


**Figure 7. Anillin's asymmetric enrichment correlates with asymmetric ingression in MDCK cells**

A) Images from an MDCK cell transiently expressing GFP-tagged anillin during cytokinesis are shown. B) A graph shows line scans of the non-ingressing (red) and ingressing (green) cortex of GFP-tagged anillin in an MDCK cell. The yellow box shows the breadth of anillin along the non-ingressing cortex, which was measured as the proportion of pixels above 50% of the maximum levels. C) A graph shows the ratio of the breadth of anillin vs. cell length for each cortex during mid and late ingression of asymmetric and symmetrically ingressing cells ($10 < n < 20$). Both fixed (stained for endogenous anillin) and live cells were used for these measurements. D) A graph shows the ratio of the breadth of anillin vs. cell length for each cortex in MDCK and Hela cells. Fixed cells were used for these measurements (n=20). The solid black bars represent average, while the dotted bars represent the standard deviations for each data set, and ** is $p < 0.01$ based on the student's t test. The scale bar is 10 μm.

Therefore, the side of cells that adhere to neighbouring cells could impart cortical forces, or changes in the distribution of proteins to negatively influence ingression.

### 3.4 E-cadherin is not asymmetrically localized in dividing MDCK cells

Adhesion between neighbouring MDCK cells occurs via E-cadherin, which forms a complex that crosslinks to intracellular F-actin and could impart forces onto the ingressing contractile ring during cytokinesis. Thus, we examined E-cadherin localization in MDCK cells during cytokinesis. In fixed MDCK cells, anillin (green) accumulated more strongly on the ingressing cortex, while E-cadherin (red) was either not enriched, or was variably enriched on the non-ingressing cortex during or just after ingression (Figure 8A). Retention or increase of E-cadherin likely reflects adhesion, while its decrease could reflect loss of adhesion. I measured the ratio of the total levels of accumulated E-cadherin and anillin on each cortex of asymmetrically ingressing cells. During mid-ingression, E-cadherin was more evenly distributed on each cortex (0.9 +/- 0.13, n=12), while anillin was more strongly enriched on the ingressing cortex (1.3 +/- 0.15). In later stages of cytokinesis, E-cadherin remained evenly distributed between each cortex (0.95 +/- 0.36; n=12), while anillin was even more enriched on the ingressing cortex (1.7 +/- 0.30, n=12; Figure 8B). This data shows that asymmetrically ingressing MDCK cells do not necessarily maintain adhesion with neighbouring cells, and reinforces our hypothesis that the core mechanism for asymmetry is intrinsic. However, we did not examine E-cadherin in symmetric cells, which could be interesting to show if enrichments on either cortex over-rides the intrinsic system.

### 3.5 Anillin is required for the asymmetric ingression of MDCK cells

Since E-cadherin was not asymmetrically distributed in asymmetrically ingressing cells, this reinforces the hypothesis that MDCK cells undergo asymmetric ingression via an intrinsic system. Since the localization of anillin correlates with asymmetric ingression, it could have a crucial role in this process. Thus, we determined how anillin depletion affects furrow ingression in MDCK cells grown in a monolayer. In anillin-depleted HeLa cells,

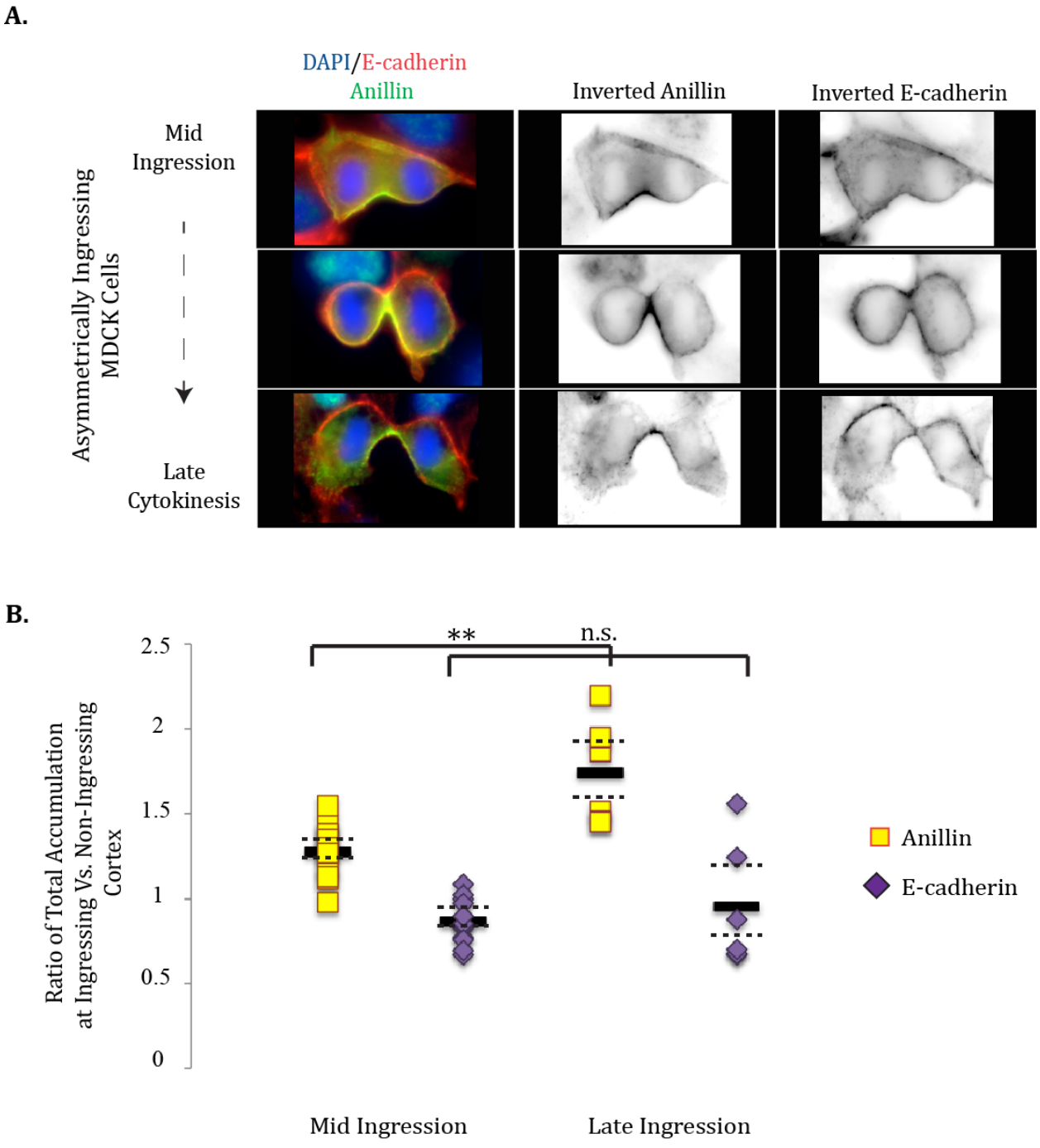


**Figure 8. E-cadherin is not asymmetrically localized in asymmetrically ingressing MDCK cells**

A) Images show z-stack projections of MDCK cells, which were fixed and stained for anillin (green) and E-cadherin (red). These images show the variability in E-cadherin levels and

distribution (low in the top cell, high on both cortices in the middle cell, and high on the non-ingressing cortex in the bottom cell). B) A graph shows the ratio of the total accumulation of E-cadherin (purple) and anillin (yellow) on each cortex in asymmetrically dividing cells during mid or late ingression (n=12). The solid black bars show the averages, while the dotted bars represent the standard deviations for each data set, and ** is $p < 0.01$ based on the student's t test.

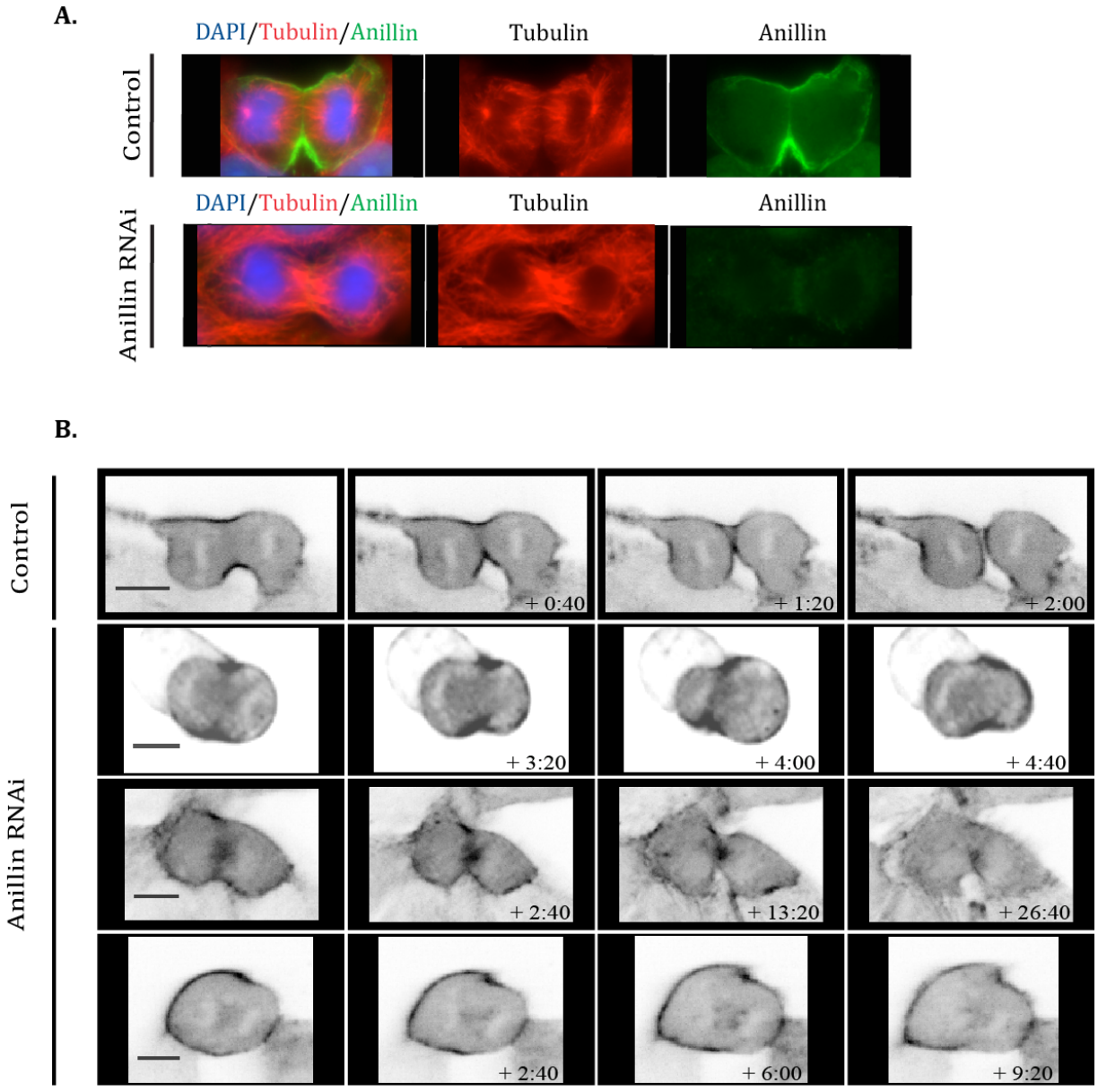
A.
DAPI/Tubulin/Anillin
Tubulin
Anillin
Control
DAPI/Tubulin/Anillin
Tubulin
Anillin
Anillin RNAi
B.
Control
Anillin RNAi
+ 0:40
+ 1:20
+ 2:00
+ 3:20
+ 4:00
+ 4:40
+ 2:40
+ 13:20
+ 26:40
+ 2:40
+ 6:00
+ 9:20

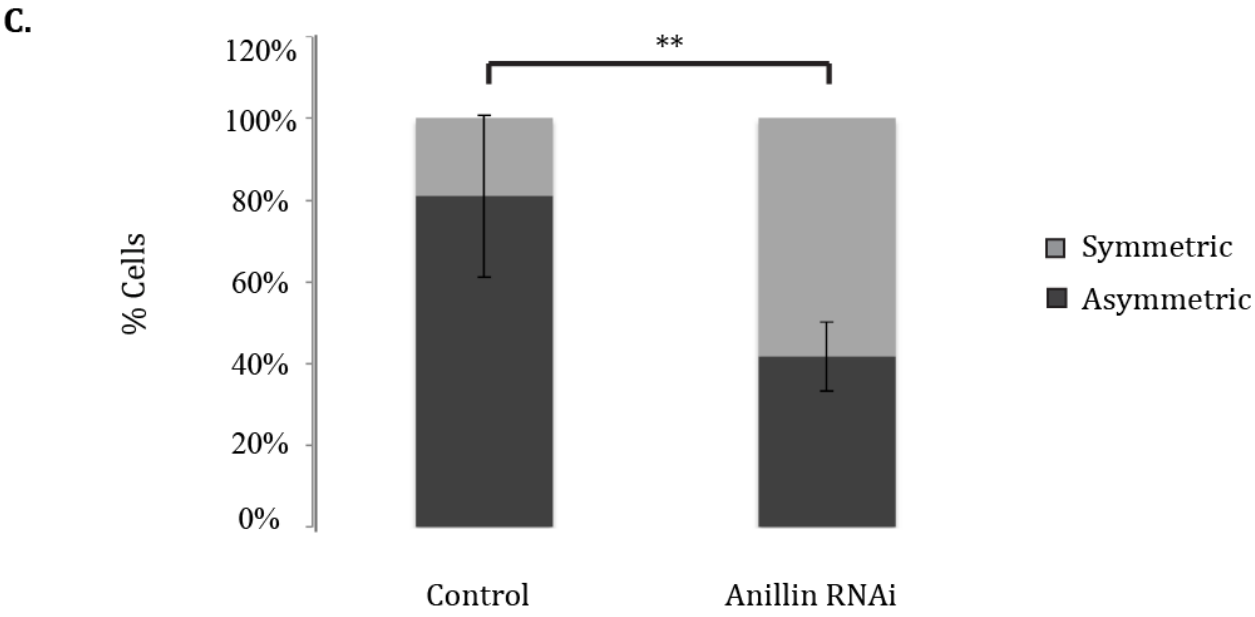


**Figure 9. Anillin is required for the asymmetric ingression of MDCK cells**

A) Images show fixed MDCK cells with or without anillin RNAi, co-stained for anillin (green), tubulin (red) and DAPI (blue). B) Images from MDCK cells stably expressing GFP:active myosin with or without anillin RNAi are shown. C) A bar graph shows the proportion of cells displaying asymmetric or symmetric ingression for control or anillin RNAi cells. The black bars show the standard deviation for each data set, and ** is $p < 0.01$ based on the student's t test. The scale bar is 10 μm.

furrow ingression begins normally, but the contractile ring oscillates around the cell for a limited period of time and cytokinesis fails (Straight et al. 2005;Piekny and Glotzer, 2008). Live imaging anillin-depleted MDCK cells stably expressing GFP:active myosin revealed that a subset of cells showed similar oscillations to HeLa cells (25%, n=8), while others failed ingression altogether (25%, n=8), or ingressed, but then later regressed (50%, n=8; Figure 8B). When examining fixed cells, I found that while 81.1 +/- 19.9% (30<n<50) of control cells showed asymmetric ingression, 58.3 +/- 8.5% of anillin-depleted cells showed symmetric ingression (Figure 9 A,C). This data suggests that anillin may be part of the intrinsic machinery that mediates asymmetric ingression.

### 3.6 Aurora B kinase inhibition does not affect asymmetric ingression

Since anillin is highly unevenly distributed along the two cortices in MDCK cells, and could be part of the pathway that mediates asymmetric ingression, we wanted to identify mechanisms that regulate anillin's localization. As described earlier, the mitotic spindle is shifted toward the apical side of epithelial cells, and previous studies showed that the central spindle and astral microtubules regulate the localization of anillin (Lewellyn et al. 2010) . Since Aurora B kinase is a key cell cycle regulator of the central spindle, and there is a gradient of Aurora B kinase activity around the central spindle, we wanted to determine if Aurora B kinase regulates anillin localization (Carmena et al., 2012). A former student in the lab found that inhibition of Aurora B kinase (with Hesperadin) caused anillin localization to shift from stabilized microtubules to the cortex in Hela cells (Figure 9A taken from Jaramillo Garcia, 2013). Thus, in MDCK cells the gradient of Aurora B kinase activity could be shifted away from one of the cortices, allowing for an increase in cortical anillin there. However, MDCK cells in monolayers are not highly polarized, and although the spindle may be shifted in these cells (Figure 9A), it may not be sufficient to maintain a large difference in Aurora B kinase activity at the two cortices. Thus, inhibiting Aurora B kinase could have two outcomes. One outcome is that anillin could increase at the non-ingressing cortex and the cells would ingress more symmetrically. Alternatively, anillin could increase at both cortices, and asymmetry would be maintained. Upon treating MDCK cells with an

Aurora B inhibitor, ZM447439, we found that the number asymmetrically ingressing cells was not statistically changed in comparison to control cells (mid-ingresssion: control 81.1% +/- 19.1% vs. 86.8% +/- 9.6%; late-ingressing: control 80.5% +/- 13.8% vs. 90.4%+/- 9.3%, 40<n<50; Figure 10B). These results suggest that in MDCK cells grown in a monolayer, an Aurora B gradient likely is not sufficient to generate the uneven distribution of anillin on the two cortices. It is not clear why anillin is distributed so unevenly, and we are currently investigating other mechanisms.

### 3.7 Ingression is variable in polarized MDCK cells

To best understand how the constraints of neighbouring cells influence ingression, MDCK cells were induced to form cysts, which are the precursors to the tubules found in the kidneys. Cysts are spherical structures with a hollow lumen found at the center (Figure 11). In order for cysts to maintain their structure, junctions are formed between neighbouring cells, and division has to occur all while maintaining this organization. In fixed cysts, we observed both symmetric and asymmetric ingression, which dependent on the location of the dividing cell (Figure 11). Therefore, in developing tissues, the ingression of cells may depend on their location, and the number of neighbours imparting extrinsic forces on the dividing cell.

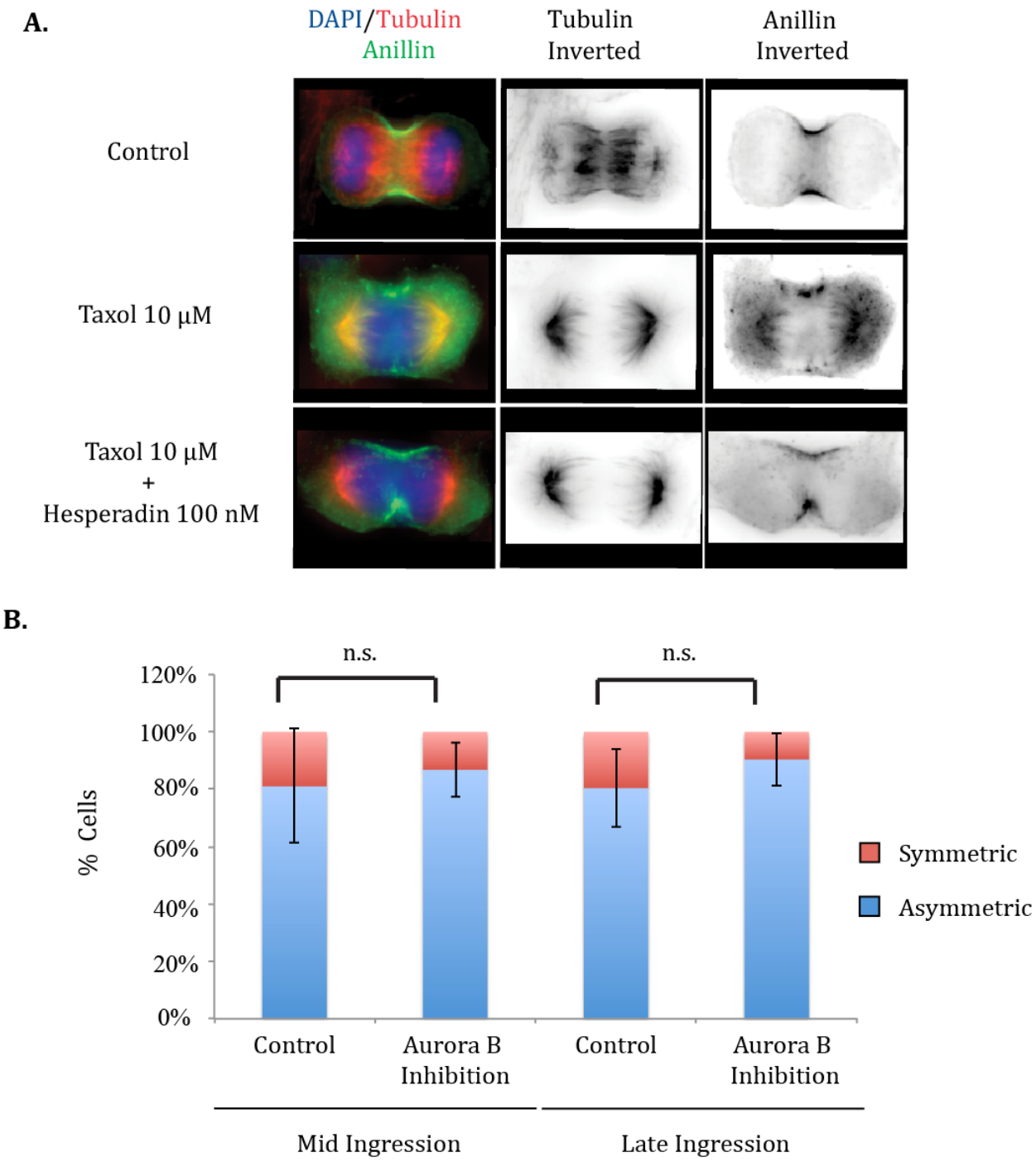


**Figure 10. Aurora B Kinase inhibition does not affect asymmetric ingression**

A) Images show z-stack projections of fixed control, taxol (10 µM) and taxol + hesperadin-treated (10 µM taxol for 20 min and 100 nM hesperadin for 30 min) Hela cells co-stained for anillin (green), tubulin (red) and DAPI (blue). *Note: adapted from the thesis of M. Jaramillo Garcia (2013).* B) A bar graph shows the percentage of control and Aurora B-

inhibited cells dividing symmetrically (red) vs. asymmetrically (blue) during mid and late ingression. The black bars show the standard deviation for each data set, and the student t test was used to test for significance.

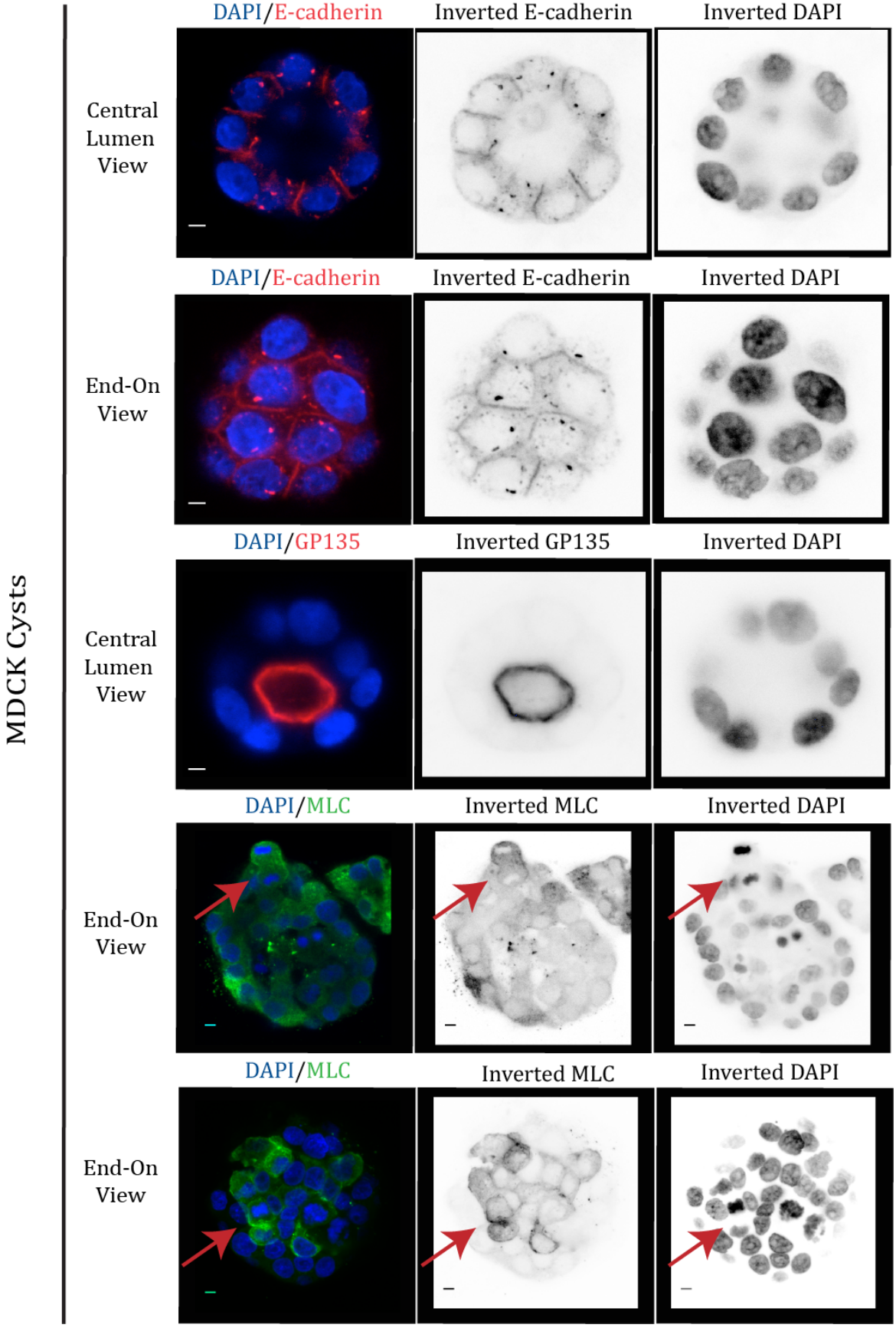
MDCK Cysts
DAPI/E-cadherin
Inverted E-cadherin
Inverted DAPI
Central Lumen View
DAPI/E-cadherin
Inverted E-cadherin
Inverted DAPI
End-On View
DAPI/GP135
Inverted GP135
Inverted DAPI
Central Lumen View
DAPI/MLC
Inverted MLC
Inverted DAPI
End-On View
DAPI/MLC
Inverted MLC
Inverted DAPI
End-On View

### Figure 11. Ingression is variable in polarized MDCK cells

Images show different z planes of projections of fixed cysts formed from MDCK cells (views are indicated). Different cysts are shown, which were co-stained for DAPI (blue) and E-cadherin, or GP135 (red), or DAPI (blue) and myosin (MLC; green). Red arrows point to dividing cells within the cysts. The scale bar is 10 μm.

# Chapter 4. Discussion

This study shows that cytokinesis can vary between different types of cultured mammalian cells. In particular, the cleavage of MDCK epithelial cells can occur asymmetrically, to a much greater extent than Hela cells. I found that extrinsic mechanisms influence the ingression of dividing epithelial cells, possibly by adhesion to neighboring cells. However, my data suggests that asymmetric ingression may also be intrinsically controlled. The mechanism for this is not clear, but may involve anillin, which is enriched on the ingressing cortex of asymmetrically ingressing cells, and is more evenly distributed in cells dividing symmetrically. Consistent with a role for anillin in asymmetric ingression, anillin RNAi causes cells to ingress more randomly, and the population of cells shifts toward ingressing more symmetrically. In cysts, cells may also ingress asymmetrically or symmetrically, depending on their location. Therefore, extrinsic forces can over-ride the intrinsic program. These data shed light on how cytokinesis is controlled within tissues, to coordinate division with the inheritance of polarity by the daughter cells.

## 4.1 Intrinsic mechanisms driving asymmetric ingression

Anillin may regulate asymmetric ingression in MDCK cells through an intrinsic mechanism. Asymmetric ingression may be an inherent property of most cells, and in multiple organisms. Even Hela cells do not ingress in a perfectly symmetrical manner, since our ratios deviated from 1, and one possibility is that the forces underlining this asymmetry could stem from the substrate that the cells are growing on (Bourdages et al. 2014). Regardless, previous studies in early *C. elegans* embryos showed that ingression of the first division occurs asymmetrically, and anillin is required for this, since its depletion caused furrow ingression to occur more symmetrically (Maddox et al. 2007). Also, MDCK cells show stronger asymmetric ingression vs. Hela cells grown on the same substrate suggesting that the substrate is not the only factor influencing asymmetric ingression. Furthermore, I observed uncoupling between anillin and active myosin in asymmetrically ingressing MDCK cells, which was not reported for Hela cells. Interestingly, I observed

enrichment of anillin on the ingressing cortex prior to anaphase entry (data not shown), and one possibility is that anillin mediates cell rounding to force the nucleus to become more apically positioned. It is not clear what causes anillin to become asymmetrically localized earlier in the cell cycle, but attractive candidates are cell cycle kinases such as Cdk1, Aurora B kinase and Polo kinase, which could be differently localized in epithelial cells vs. other cell types. It is also not clear how anillin can modulate changes in the ingressing cortex when active myosin is not enriched in the same location. Interestingly, septins are another filament system that bind to anillin, and have been implicated in polarity and cell shape change events. Septins are conserved GTP-binding proteins that concentrate in the contractile ring and regulate asymmetric ingression in *C. elegans* embryos (Maddox et al. 2007). In budding yeast, septins are one of the first proteins to mark the site of the future daughter bud in interphase, where the filaments are thought to form a diffusion barrier that can selectively partition the cytosol and membrane near the forming daughter bud (York et al. 2000; Barral et al. 2000). Little is known about the function of septin filaments, and if they can influence the cortex independently of the actomyosin or microtubule cytoskeletons. Our future directions will involve studying the localization of septins in asymmetrically ingressing MDCK cells to determine if they are also enriched on the ingressing cortex, and if depletion of anillin alters their localization.

### 4.2 Extrinsic mechanisms influence ingression

My evidence suggests that extrinsic mechanical forces by adhesion to multiple neighbouring cells can over-ride the intrinsic system and cause epithelial cells to ingress more symmetrically. MDCK cells in cysts ingress asymmetrically or symmetrically, depending on their location, suggesting that highly polarized cells rely on multiple mechanisms for ingression. Epithelial cells express E-cadherin, which is part of a complex that forms adherens junctions with neighbouring cells, and connects to intracellular F-actin (Sandquist and Bement 2010; P. D. Goldbach 2011; Takeichi 2014). Previous studies in *Drosophila* epithelial tissue showed that apically-enriched E-cadherin complexes drive the polarized constriction of the contractile ring from the basal plane towards the apical plane of the cell, suggesting that forces generated through these junctions directly influence the

contractile ring (Morais-de-Sá and Sunkel 2013; Guillot and Lecuit 2013). During division, adherens junctions and the contractile ring each impart forces on the dividing cell. Initially, the forces generated through intact junctions could cause the apical cortex to be less pliable than the basal cortex. However, once the tension in the contractile ring outcompetes the tension at the junctions, they disengage and the apical cortex ingresses (Founounou, Loyer, and Le Borgne 2013; Guillot and Lecuit 2013). The disengagement of junctions depends on tension and the number of neighbouring cells, since an increased number of neighbours surrounding the dividing cell delays junction disengagement (Guillot and Lecuit 2013).

We also found that multiple neighbours could over-ride asymmetric ingression when MDCK cells were grown as monolayers, suggesting that adhesion in general could influence forces associated with the contractile ring. It is not clear how this adhesion could influence intracellular F-actin and over-ride intrinsic mechanisms for ingression. In *Drosophila* spermatocytes, the overexpression of E-cadherin in anillin-depleted cells suppressed cytokinesis defects, and they proposed that E-cadherin stabilized F-actin in the contractile ring, suggesting that multiple mechanisms could crosslink F-actin and myosin to the plasma membrane (P. Goldbach et al. 2010). In MDCK cells, we found that E-cadherin was randomly distributed on the non-ingressing and ingressing cortices of asymmetrically ingressing cells. However, we need to determine if E-cadherin is enriched on one of the cortices in symmetrically ingressing cells, and test how altering the levels of E-cadherin affect ingression.

## References


Akhshi, Tara Kafiyeh, Denise Wernike, and Alisa Piekny. 2013. "Microtubules and Actin Crosstalk in Cell Migration and Division." *Cytoskeleton (Hoboken, N.J.)* 71 (1): 1–23. doi:10.1002/cm.21150.

Barral, Yves, Valerie Mermall, Mark S Mooseker, and Michael Snyder. 2000. "Compartmentalization of the Cell Cortex by Septins Is Required for Maintenance of Cell Polarity in Yeast." *Molecular Cell* 5 (5): 841–51. doi:10.1016/S1097-2765(00)80324-X.

Bourdages, Karine G, Benjamin Lacroix, Jonas F Dorn, Carlos P Descovich, and Amy S Maddox. 2014. "Quantitative Analysis of Cytokinesis In Situ during C. Elegans Postembryonic Development." *PloS One* 9 (10): e110689. doi:10.1371/journal.pone.0110689.

Bryant, David M, and Keith E Mostov. 2008. "From Cells to Organs: Building Polarized Tissue." *Nature Reviews. Molecular Cell Biology* 9 (11): 887–901. doi:10.1038/nrm2523.

Chung, Seyeon, and Deborah J Andrew. 2008. "The Formation of Epithelial Tubes." *Journal of Cell Science* 121 (Pt 21): 3501–4. doi:10.1242/jcs.037887.

Floyd, Suzanne, Nicola Whiffin, Maria P Gavilan, Stefan Kutscheidt, Maria De Luca, Chiara Marcozzi, Mingwei Min, et al. 2013. "Spatiotemporal Organization of Aurora-B by APC/CCdh1 after Mitosis Coordinates Cell Spreading through FHOD1." *Journal of Cell Science* 126 (Pt 13): 2845–56. doi:10.1242/jcs.123232.

Founounou, Nabila, Nicolas Loyer, and Roland Le Borgne. 2013. "Septins Regulate the Contractility of the Actomyosin Ring to Enable Adherens Junction Remodeling during Cytokinesis of Epithelial Cells." *Developmental Cell* 24 (3). Elsevier Inc.: 242–55. doi:10.1016/j.devcel.2013.01.008.

Fuller, Brian G. 2010. "Self-Organization of Intracellular Gradients during Mitosis." *Cell Division* 5 (1): 5. doi:10.1186/1747-1028-5-5.

Glotzer, Michael. 2009. "NIH Public Access." *Nature Reviews. Molecular Cell Biology* 10 (1): 9–20. doi:10.1038/nrm2609.The.

Goldbach, Philip Daniel. 2011. "Anillin Stabilizes Membrane-Cytoskeleton Interactions During Drosophila Male Germ Cell Cytokinesis by Anillin Stabilizes Membrane-Cytoskeleton Interactions During."

Goldbach, Philip, Raymond Wong, Nolan Beise, Ritu Sarpal, William S Trimble, and Julie a Brill. 2010. "Stabilization of the Actomyosin Ring Enables Spermatocyte Cytokinesis in

Drosophila." *Molecular Biology of the Cell* 21 (9): 1482–93. doi:10.1091/mbc.E09-08-0714.

Green, Rebecca a, Ewa Paluch, and Karen Oegema. 2012. "Cytokinesis in Animal Cells." *Annual Review of Cell and Developmental Biology* 28 (January): 29–58. doi:10.1146/annurev-cellbio-101011-155718.

Guillot, Charlène, and Thomas Lecuit. 2013. "Adhesion Disengagement Uncouples Intrinsic and Extrinsic Forces to Drive Cytokinesis in Epithelial Tissues." *Developmental Cell* 24 (3): 227–41. doi:10.1016/j.devcel.2013.01.010.

Hutterer, Andrea, Michael Glotzer, and Masanori Mishima. 2009. "Europe PMC Funders Group Clustering of Centralspindlin Is Essential for Its Accumulation to the Central Spindle and the Midbody." *Current Biology* 19 (23): 2043–49. doi:10.1016/j.cub.2009.10.050.Clustering.

Leung L, Klopper AV, Grill SW, Harris WA, Norden C. "Apical migration of nuclei during G2 is a prerequisite for all nuclear motion in zebrafish neuroepithelia". *Development (Cambridge, England)* 138 (22): 5003-5013. doi:10.1242/dev.071522.

Lewellyn, Lindsay, Julien Dumont, Arshad Desai, and Karen Oegema. 2010. "Analyzing the Effects of Delaying Aster Separation on Furrow Formation during Cytokinesis in the Caenorhabditis Elegans Embryo." *Molecular Biology of the Cell* 21 (1): 50–62. doi:10.1091/mbc.E09-01-0089.

Maddox, Amy Shaub, Lindsay Lewellyn, Arshad Desai, and Karen Oegema. 2007. "Anillin and the Septins Promote Asymmetric Ingression of the Cytokinetic Furrow." *Developmental Cell* 12 (5): 827–35. doi:10.1016/j.devcel.2007.02.018.

Martin-Belmonte, Fernando, and Keith Mostov. 2008. "Regulation of Cell Polarity during Epithelial Morphogenesis." *Current Opinion in Cell Biology* 20 (2): 227–34. doi:10.1016/j.ceb.2008.01.001.

Meyer, Emily J, Aissam Ikmi, and Matthew C Gibson. 2011. "Interkinetic Nuclear Migration Is a Broadly Conserved Feature of Cell Division in Pseudostratified Epithelia." *Current Biology : CB* 21 (6): 485–91. doi:10.1016/j.cub.2011.02.002.

Morais-de-Sá, Eurico, and Claudio Sunkel. 2013. "Adherens Junctions Determine the Apical Position of the Midbody during Follicular Epithelial Cell Division." *EMBO Reports* 14 (8): 696–703. doi:10.1038/embor.2013.85.

Morin, Xavier, and Yohanns Bellaïche. 2011. "Mitotic Spindle Orientation in Asymmetric and Symmetric Cell Divisions during Animal Development." *Developmental Cell* 21 (1): 102–19. doi:10.1016/j.devcel.2011.06.012.

Nakajima, Yu-ichiro, Emily J Meyer, Amanda Kroesen, Sean a McKinney, and Matthew C Gibson. 2013. "Epithelial Junctions Maintain Tissue Architecture by Directing Planar Spindle Orientation." *Nature* 500 (7462). Nature Publishing Group: 359–62. doi:10.1038/nature12335.

Peyre, Elise, Florence Jaouen, Mehdi Saadaoui, Laurence Haren, Andreas Merdes, Pascale Durbec, and Xavier Morin. 2011. "A Lateral Belt of Cortical LGN and NuMA Guides Mitotic Spindle Movements and Planar Division in Neuroepithelial Cells." *The Journal of Cell Biology* 193 (1): 141–54. doi:10.1083/jcb.201101039.

Piekny, Alisa J, and Michael Glotzer. 2008. "Anillin Is a Scaffold Protein That Links RhoA, Actin, and Myosin during Cytokinesis." *Current Biology : CB* 18 (1): 30–36. doi:10.1016/j.cub.2007.11.068.

Piekny, Alisa, Michael Werner, and Michael Glotzer. 2005. "Cytokinesis: Welcome to the Rho Zone." *Trends in Cell Biology* 15 (12): 651–58. doi:10.1016/j.tcb.2005.10.006.

Ragkousi, K., and M. C. Gibson. 2014. "Cell Biology in Development: Cell Division and the Maintenance of Epithelial Order." *The Journal of Cell Biology* 207 (2): 181–88. doi:10.1083/jcb.201408044.

Reinsch, S. 1994. "Orientation of Spindle Axis and Distribution of Plasma Membrane Proteins during Cell Division in Polarized MDCKII Cells." *The Journal of Cell Biology* 126 (6): 1509–26. doi:10.1083/jcb.126.6.1509.

Sandquist, Joshua C, and William M Bement. 2010. "Hold on Tightly, Let Go Lightly: Myosin Functions at Adherens Junctions." *Nature Cell Biology* 12 (7). Nature Publishing Group: 633–35. doi:10.1038/ncb0710-633.

Spear, Philip C and Erickson, Carol A. 2012. "NIH Public Access." *Developmental Biology* 370 (1): 33–41. doi:10.1016/j.ydbio.2012.06.031.Apical.

Straight, Aaron F, Christine M Field, and Timothy J Mitchison. 2005. "Anillin Binds Nonmuscle Myosin II and Regulates the Contractile Ring □." *Molecular Biology of the Cell* 16 (January): 193–201. doi:10.1091/mbc.E04.

Takeichi, Masatoshi. 2014. "Dynamic Contacts: Rearranging Adherens Junctions to Drive Epithelial Remodelling." *Nature Reviews. Molecular Cell Biology* 15 (6). Nature Publishing Group: 397–410. doi:10.1038/nrm3802.

Tepass, Ulrich. 2012. "The Apical Polarity Protein Network in Drosophila Epithelial Cells: Regulation of Polarity, Junctions, Morphogenesis, Cell Growth, and Survival." *Annual Review of Cell and Developmental Biology* 28 (January): 655–85. doi:10.1146/annurev-cellbio-092910-154033.

York, New, Peter A Takizawa, Joseph L Derisi, James E Wilhelm, and Ronald D Vale. 2000. "Plasma Membrane Compartmentalization in Yeast by Messenger RNA Transport and a Septin Diffusion Barrier." *Science (New York, N.Y.)* 290 (October): 341–45.